



NTNU – Trondheim
Norwegian University of
Science and Technology

Drag and Wake Measurements on Cylinders and Discs for Wind Turbine Wake Modelling

Paul Wilpert

Master's Thesis

Submission date: June 2014

Supervisor: Lars Sætran, EPT

Norwegian University of Science and Technology
Department of Energy and Process Engineering



NTNU – Trondheim
Norwegian University of
Science and Technology

Drag and Wake Measurements on Cylinders and Discs for Wind Turbine Wake Modelling

Paul Wilpert

16. June 2014

MASTER THESIS

Department of Energy and Process Engineering
Norwegian University of Science and Technology

Supervisor 1: Lars Roar Sætran

Supervisor 2: Jan Bartl

Abstract

This master thesis presents an experimental study of the mean wake velocities, the drag coefficients and the vortex frequencies behind cylinders, porous discs and circular full discs. The thesis contributes to the development and better understanding of simple wind turbine wake models. The future long term goal is to improve the complex fluid flow models of wind turbines.

The experimental trials were executed in two different wind tunnels at the Energy and Process Engineering Department of NTNU. The main trials have been conducted to determine the drag coefficient with two independent methods. Pitot tubes were used to determine the mean wake velocities and the drag coefficients by using the measurement by wake method. Furthermore, the force survey method was established by using a force plate. A broad literature survey revealed a consistent range of drag coefficients and mean wake velocities comparable to the determined results of the current investigation. Additionally it was found, that the measured upstream flow velocity has a major influence on the measurement by wake method. The results of the force survey method gave strong evidence, that the blockage effect has a negative influence.

The final experiments were conducted as additional study on wake flows. The method applied was based on hot wire velocity measurements to determine the vortex shedding frequencies. A literature review predicted the vortex shedding frequencies of cylinders and circular full discs in a comparable range of the experimental results shown by the power spectral density analysis. The analysis of the porous biplane disc unfolded no discrete frequency.

A comparison of the results of the mean wake flows revealed a significant variation between shape of the cylinder and discs to the model wind turbine. However, the porous monoplane disc achieved the best results and is therefore most promising for future investigations on wind turbine wake modelling.

Affidavit

I hereby declare that I wrote the thesis on my own without any assistance from a third party. I confirm that no sources have been used other than those clearly marked as other sources. This thesis has not been received by any examination board, neither in this nor in a similar form.

Trondheim, June 16th, 2014

A handwritten signature in blue ink, appearing to read "P. Wilper", is written below the date.

Acknowledgment

I would like to thank the following persons for their great help during my work on this thesis. First of all my closest working partner, supervisor and somebody who was always available when I needed help: Jan Bartl. He introduced me to the subject and pushed me in the right direction when I was in danger of losing track. I want to thank him for many constructive talks and meetings.

Besides I also want to thank my supervisor Lars Roar Sætran. He helped me with a lot of official obstacles, but also showed me and Jan from time to time opportunities we did not see.

I am really thankful for the monetary support by the PROMOS scholarship, the Berlin Institute of Technology and also the Energy and Process Engineering Department of NTNU in Trondheim. My thesis at NTNU would not have been possible without the financial aid of these sources.

I had a great time in Trondheim and at NTNU and I hope that many students and PHD candidates get the same opportunities.

P.W.

Contents

1	Introduction	1
1.1	Background	1
1.2	Problem Formulation and Objectives	2
2	Aerodynamic Fundamentals	3
2.1	Non-dimensional Numbers	3
2.2	Drag Force and Drag Coefficient	5
2.3	Drag Measurement by Wake and Force Survey Method	6
2.4	Flow around a Cylinder	7
2.5	Vortex Shedding on a Cylinder	10
2.6	Porous Discs - Grids of Finite Extension	11
2.7	Circular Full Disc	13
2.8	Actuator Disc Model	15
2.9	Model Wind Turbine Wake	17
3	Measurement Methods	18
3.1	NTNU Wind Tunnels	18
3.2	Force Measurement	20
3.2.1	Strain Gages	20
3.2.2	Force Plate	21
3.3	Velocity and Pressure Measurements	23
3.3.1	Pitot Tube	23
3.3.2	Contraction	24

CONTENTS

3.3.3	Pressure Transducers	25
3.3.4	Hot Wire Anemometry	25
3.4	Instrument Calibrations	27
3.4.1	Pitot Tube and Contraction	27
3.4.2	Hot Wire Anemometer	28
3.5	Cylinder, Porous Monoplane and Circular Full Disc Design	30
4	Experimental Results	32
4.1	Preparatory Work	32
4.1.1	Aerodynamic Forces	32
4.1.2	Cylinder Vortex Shedding	33
4.2	Static Cylinder Measurement	34
4.2.1	Goal of Experiment	34
4.2.2	Experimental Set-up	34
4.2.3	Results	35
4.2.4	Conclusions	37
4.3	Static Porous Monoplane and Circular Full Disc Measurements	38
4.3.1	Goal of Experiment	38
4.3.2	Experimental Set-up	38
4.3.3	Results	39
4.3.4	Conclusions	46
4.4	Vortex shedding in the Wake of Cylinder, Porous Monoplane and Circular Full Disc	47
4.4.1	Goal of Experiment	47
4.4.2	Experimental Set-up	47
4.4.3	Results	48
4.4.4	Conclusions	51
4.5	Error analysis	52
4.5.1	Pitot Tube Measurements	52
4.5.2	Hot Wire Measurements	53

CONTENTS

4.6 Comparison of Mean Wake Flows	55
5 Summary and Conclusions	57
Appendix	I
A Additional tables	I
Bibliography	VII

List of Figures

2.1	Drag coefficients for different bodies	5
2.2	Control volume over the length of test section	6
2.3	Regimes of flow around a smooth, circular cylinder	7
2.4	Flow behind a cylinder	8
2.5	Correlation of drag coefficient and Reynolds number for cylinders	8
2.6	Strouhal number trend dependent on the Reynolds number for cylinders	10
2.7	Mean velocities measured behind a porous monoplane disc	11
2.8	Flow behind a circular full disc for different distances	13
2.9	Drag coefficients for circular flat plates	14
2.10	Actuator disc model of a wind turbine	15
2.11	Model wind turbine mean wake velocity distribution	17
3.1	Big and small NTNU wind tunnel	19
3.2	Strain gages	20
3.3	Coordinate system of force plate	22
3.4	Principal structure of a Pitot tube	23
3.5	Venturi tube	24
3.6	Principal circuit of a constant temperature hot wire anemometer	26
3.7	Pitot tube calibration curve, with best-fit line and equation	27
3.8	Hot wire anemometer calibration curve, with best-fit line and equation	29
3.9	Investigated bodies	30
4.1	Wind tunnel arrangement for cylinder wake measurement	34

LIST OF FIGURES

4.2 Mean velocity allocation behind the cylinder and a asymptotic velocity . . . 35

4.3 Non-dimensional mean velocity allocation for the cylinder compared to Ong and Wallace 36

4.4 Wind tunnel arrangement for full drag disc and porous monoplane disc wake measurement 38

4.5 Vertical velocity allocation behind the porous monoplane and the circular full disc 39

4.6 Horizontal velocity allocation behind the porous monoplane and the circular full disc 40

4.7 Comparison porous monoplane disc measurements with Pierella and Sætran 41

4.8 Comparison of full disc measurements with measurements of Cannon . . . 42

4.9 Velocity allocation of rotational wake behind a porous monoplane disc and a circular full disc 43

4.10 Velocity allocation in front of the full drag disc center with growing distance . 44

4.11 Velocity allocation 30 cm in front and directly aside the full drag disc 45

4.12 Wind tunnel arrangement for vortex shedding analysis 47

4.13 Time series and power spectral density for the cylinder 49

4.14 Time series and power spectral density for the porous biplane disc 50

4.15 Time series and power spectral density for the circular full disc 51

4.16 Mean wake flow comparison in 5 D distance of cylinder, porous monoplane disc, circular full disc and model wind turbine by Bartl 55

List of Tables

4.1	Estimated aerodynamic dimensions	33
4.2	Estimated vortex frequencies	33
4.3	Comparison of determined drag coefficients	43
4.4	Hot wire calibration and set-up	48
A.1	Pressure and velocity in cylinder wake	I
A.2	Pressure and velocity in cylinder wake	II
A.3	Pressure and velocity in the horizontal wake of the porous monoplane and full drag disc	III
A.4	Pressure and velocity in the vertical wake of the full drag and porous mono- plane disc	IV

Symbols

Latin letters		
A	Surface	[m ²]
C_D	Drag coefficient	[-]
C_P	Power coefficient	[-]
D	Diameter	[m]
e	Error	[-]
f	Vortex frequency	[1/s], [Hz]
F	Hot wire factor	[-]
F_c	Adapted drag coefficient	[-]
F_D	Drag force	[N]
F_m	Measured drag coefficient	[-]
$F_{x,y,z}$	Force vector	[N]
g	Gravitational acceleration	[m/s ²]
k	Angel quotient	[-]
k	Adaptation factor	[-]
l	Length	[m]
m	Mass	[kg]
$M_{x,y,z}$	Moments	[Nm]
p	Pressure	[Pa]
P	Power	[W]
R	Radius	[m]
R	Electrical resistance	[Ω]
Re	Reynolds number	[-]
S	Body surface	[m ²]
St	Strouhal number	[-]
t	Time	[s]
T	Temperature	[°C]
u	Velocity	[m/s]
U	Voltage	[V]
U^*	Dimensionless velocity	[-]
x	X-position	[m]
y	Y-position	[m]
z	Height	[m]

Symbols

Greek letters

α	Heat transfer coefficient	[W/(m ² ·K)]
ν	Kinematic viscosity	[m ² /s]
ρ	Density	[kg/m ³]
σ	Porosity	[-]

Chapter 1

Introduction

1.1 Background

Fossil fuels provide most of the primary energy in the world. The carbon dioxide emissions of conveying, transportation and conversion are hazardous for the environment and humans. Additionally a limited availability and increasing prices make the use of renewable energies interesting. The goal of our generation is to enlarge the sustainable energy production to reduce emissions and pollution.

As an important pillar of renewable energies, the wind power capacity was growing by 18.9 % in 2012 and contributes a quote of 2.3 % of the total electricity production world wide [3]. But wind power faces more and more difficulties in western countries e.g. allocation of uneconomic regions and a growing resistance in the population. Thus only a few opportunities are left to increase the energy output in dense populated regions like Europe. Repowering for example is a successful approach to replace many old by a few new wind turbines. As well as in new wind farms, knowledge and experience was used to create more efficient wind turbines and wind farms. This is mostly based on model approaches, which are developed and analysed with computers or experiments. Computational fluid dynamic (CFD) models and wind tunnel experiments give good opportunities to investigate appearing real life situations according to mechanical and aerodynamical conditions. But even today with good CFD programs are wind tunnel experiments for many applications indispensable. They are necessary to understand complex structures and to validate or

create models, that help to increase efficiency of wind farms.

The Energy and Process Department of NTNU is investigating on model wind turbine wake measurements in controlled wind tunnel environments, that serve verification of different CFD wake models. Krogstad and Eriksen [9] focus on wake measurements of a model wind turbine. The work was continued by Pierella et al. [18], who analysed the wake development of two in-line model wind turbines.

A way to simplify turbine wake models could be the use of porous and circular full disc wakes. The first step is to compare the mean wake flows of circular discs and model wind turbines. This thesis focusses on mean velocity distribution and vortex shedding in the wake of cylinders and circular discs.

1.2 Problem Formulation and Objectives

The goal of the proposed Master thesis is to measure mean wake velocities and vortices behind cylinders and circular discs as well as the determination of drag coefficients. Additionally shall suitable measurement devices for occurring velocities and forces be evaluated and selected. Also the investigation of appearing physical effects and suitable formulas have to be found and set into account to the requirements of the experimental design. Appropriate literature research is the main basis to make feasible choices with the view on design, structures and assemblies. Also a possible comparability and confirmability of the results is aspired.

The basic idea is to measure wake flows and appearing forces of aerodynamic models for example cylinders and circular full discs. The performance of cylinders and circular full discs in a flow channel have been investigated for many years in a lot of surveys and shall be compared to wake measurements.

The main objectives of this Master's project are

1. Measurements of drag forces and mean wake velocities
2. Comparison of the drag measurement by wake and force survey method
3. Assessment of vortex shedding frequencies in cylinder and disc wakes

Chapter 2

Aerodynamic Fundamentals

This chapter is based on literature research and will handle the identification of the main phenomena regarding fluid and mechanical engineering. First of all are dimensionless numbers introduced, before presenting the drag force and drag coefficient. The sections of cylinder, circular full disc and porous discs are handling appearing aerodynamical phenomena and introducing previous investigations. This is necessary to validate and compare later experiment measurements. The last part of this chapter is an introduction of the actuator disc model and a mean wake velocity measurement of a model wind turbine.

2.1 Non-dimensional Numbers

Reynolds Number

The idea of the Reynolds number Re is the comparison of flows around geometrical similar bodies. The comparison includes different fluids, velocities and sizes of compared bodies. The Reynolds number is defined as the quotient of inertial forces to viscous forces in liquids and gasses. It is dependent on the flow speed u , the characteristic linear dimension l and the kinematic viscosity ν .

$$Re = \frac{u \cdot l}{\nu} \quad (2.1)$$

Depending on the bodies, can the flows be distributed into laminar and turbulent flows by the range of the Reynolds number. The Reynolds number is used in a wide range

CHAPTER 2. AERODYNAMIC FUNDAMENTALS

of engineering application and also often given as reference for other quantities, that are dependent on the flow regime. [22, p. 4 f]

Strouhal Number

The Strouhal number St is significant to characterize unsteady flow e.g. the vortex shedding frequency of cylinders. It can be defined with the vortex frequency f , the diameter d of the body and the velocity u of the fluid:

$$St = \frac{f \cdot D}{u} \quad (2.2)$$

Especially interesting is the Strouhal number for cylinders, which is about 0.2 for a certain range of Reynolds numbers. This will be further introduced in section 2.4. [24, p. 85 f] [25, p. 10]

2.2 Drag Force and Drag Coefficient

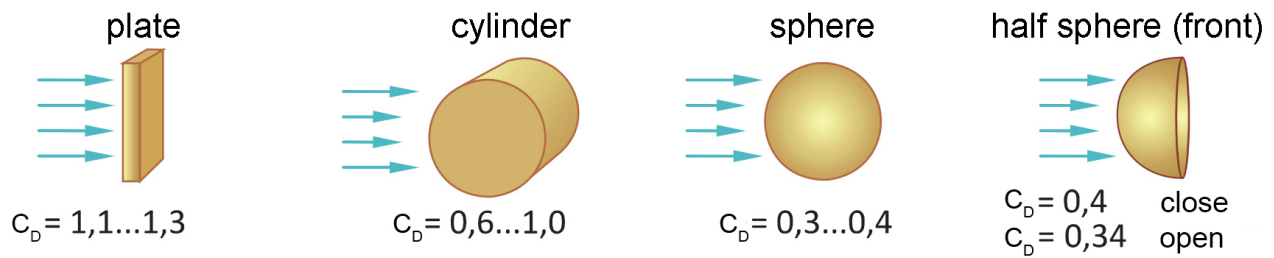


Figure 2.1: Drag coefficients for different bodies [19, p. 249]

All wind exposed objects, that have a surface orthogonal to the flow direction, are affected by the drag force F_D . It is dependent on the wind velocity u , the fluid density ρ , the surface in the wind and the drag coefficient C_D :

$$F_D = C_D \cdot \frac{1}{2} \cdot \rho \cdot A \cdot u^2 \quad (2.3)$$

The drag coefficient is dependent on the body shape and usually constant for a wide range of Reynolds numbers. Some coefficient examples for different Reynolds ranges can be seen in figure 2.1, but many more can be found in various literature. [19, p. 249]

2.3 Drag Measurement by Wake and Force Survey Method

The drag coefficient for cylinders can be indirectly determined by using the integral momentum equation. As shown in figure 2.2 is the up and downstream flow of the target object analysed. Due to symmetry can this be handled as a two dimensional problem. The uniform upstream flow moves around the cylinder and changes the pressure and speed allocation in the downstream flow. The downstream flow allocation can be seen in figure 2.2 on the right side.

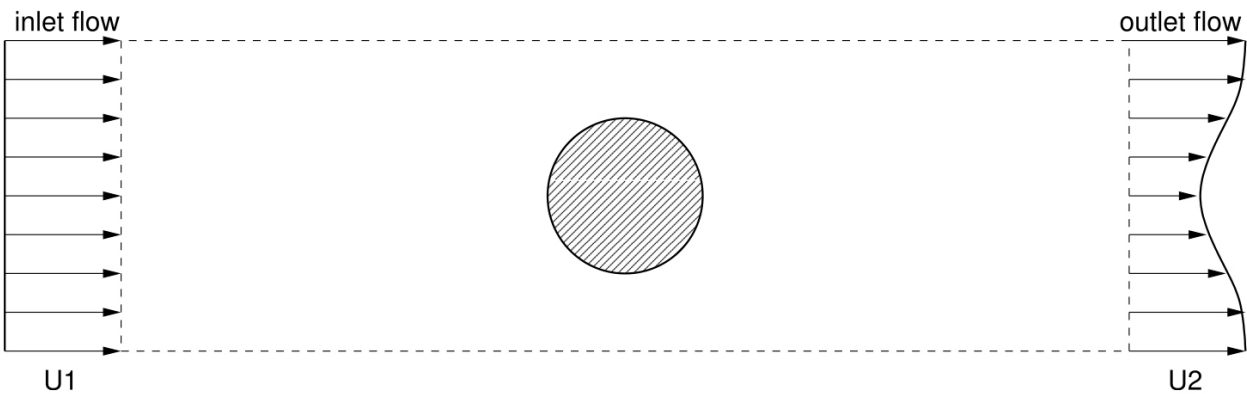


Figure 2.2: Control volume over the length of test section [4, p. 10]

White [29] give the following equation for the drag force, which is dependent on the density ρ , the upstream velocity u_1 , the downstream velocity $u_2(y)$ dependent on the position y and the length l of the cylinder.

$$F_D = \rho u_1^2 \int_{-h}^h \frac{u_2(y)}{u_1} \left(1 - \frac{u_2(y)}{u_1} \right) l dy \quad (2.4)$$

The drag coefficient is given in dependency of the drag force and the diameter of cylinder D :

$$C_D = \frac{F_D}{0.5 \rho u_1^2 A} \quad (2.5)$$

Contrary to the indirect method can the drag coefficient be determined by measuring the drag force directly. A possible measure set-up can be a force platform. Further details about operation and features will be presented in chapter 3.2.2. [29, p. 453ff][21]

2.4 Flow around a Cylinder





	No separation. Creeping flow	$Re < 5$
	A fixed pair of symmetric vortices	$5 < Re < 40$
	Laminar vortex street	$40 < Re < 200$
	Wake completely turbulent.	$300 < Re$ Critical

Figure 2.3: Regimes of flow around a smooth, circular cylinder (Adapted from Sumer and Fredsoe [25, p. 2])

The flow regime around a cylinder is dependent on the Reynolds number presented in section 2.1. The characteristic length for cylinders is the diameter D . As seen in figure 2.3 the wake flow changes from no separation for small Reynolds numbers to different vortex flows for increasing Reynolds numbers. In the range of $40 < Re < 200$ is a laminar vortex street developing, before the vortex becomes turbulent with rising Reynolds numbers.

The wake flow of a cylinder was investigated by Ong and Wallace [16] and is shown for different distances in figure 2.4. It can be seen that the velocity directly behind the cylinder is the lowest. Additionally is the lowest velocity point for the $3D$ distance lower than for the $5D$ and $10D$ distances. The far wake flow velocities, left and right, are as high as the inlet velocity. [16, p. 447ff]

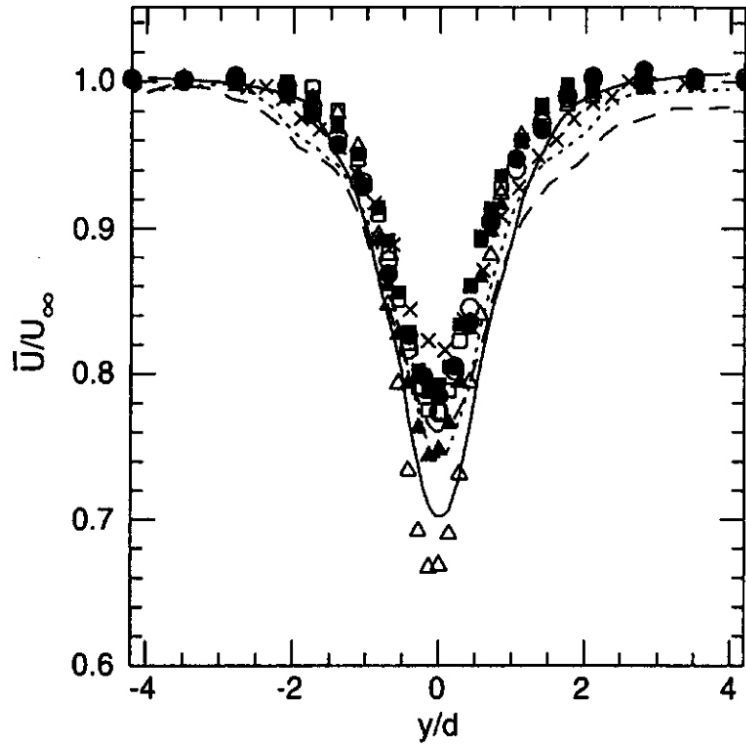


Figure 2.4: Mean velocity field behind a cylinder in different distances e.g. Δ : $3 D$, \square : $5 D$, \times : $10 D$ (Adapted from Ong and Wallace [16, p. 447])

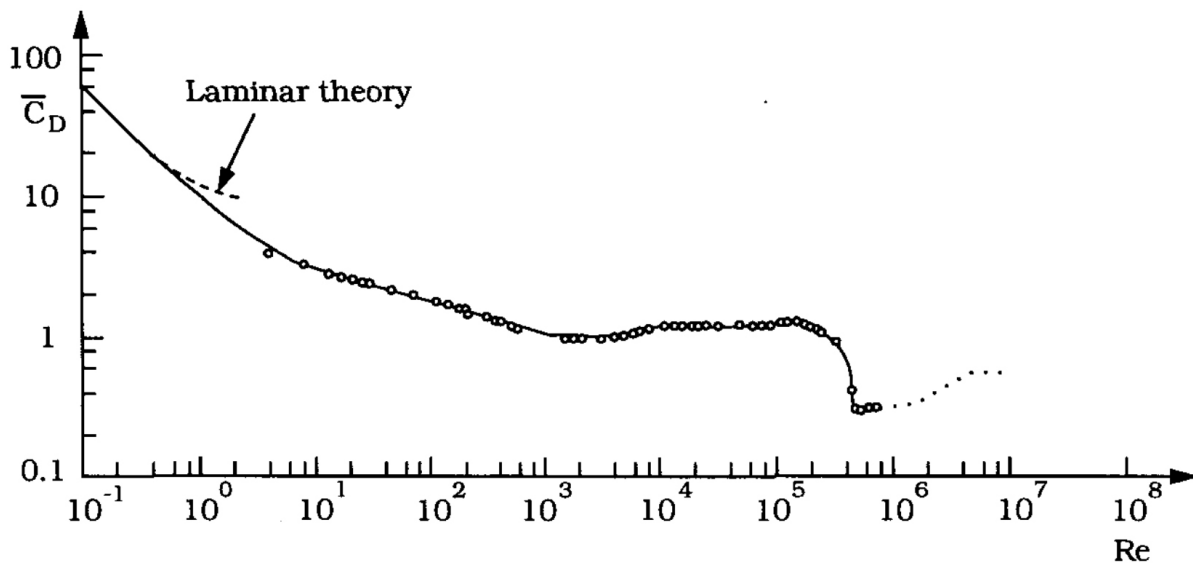


Figure 2.5: Correlation of drag coefficient and Reynolds number for cylinders [25, p. 43]

CHAPTER 2. AERODYNAMIC FUNDAMENTALS

The drag coefficient development for a smooth cylinder in dependency of the Reynolds number can be seen in figure 2.5. The C_D is big for small Reynolds numbers and decreases until $Re = 300$. For the range $300 < Re < 3 \cdot 10^5$ is C_D given as 1.2, before it decreases dramatically. [25, p. 43ff]

2.5 Vortex Shedding on a Cylinder

Vortex shedding appears for $Re > 40$ due to the development of a vortex street in the wake of cylinders. Sumer and Fredsoe [25, p. 6] basically described the mechanism in the following way: "... , the boundary layer over the cylinder surface will separate due to the adverse pressure gradient imposed by the divergent geometry of the flow environment at the rear side of the cylinder." In addition to the movement of the flow appears delamination, while the effect described by Sumer and Fredsoe [25, p. 6] affects the adverse side. [25, p. 1 ff]

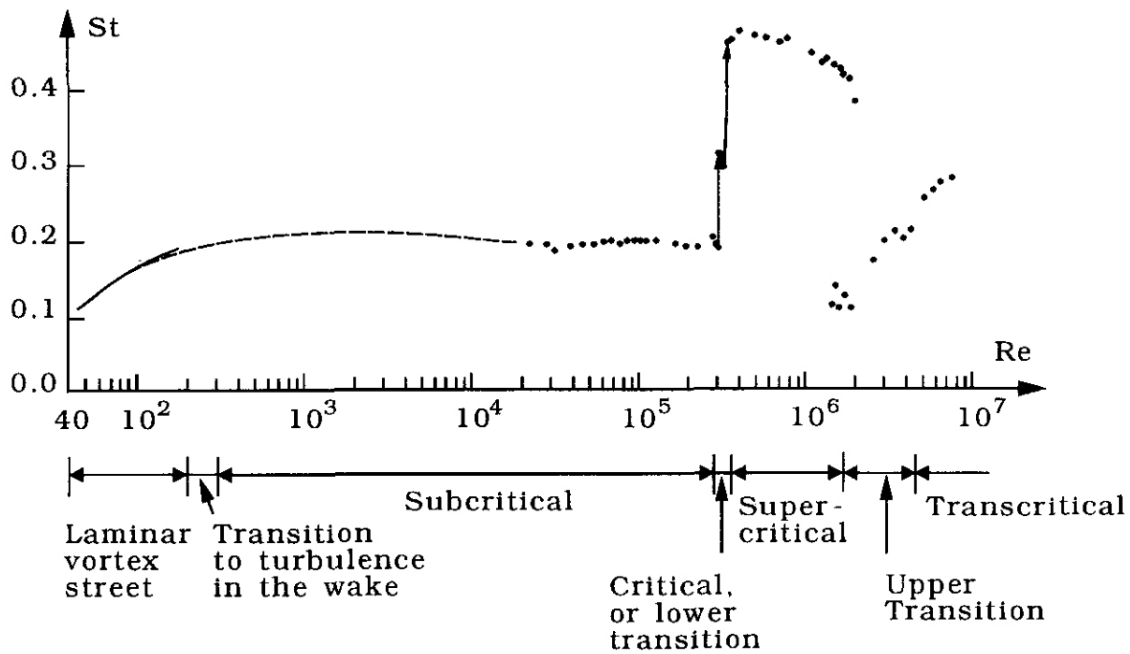


Figure 2.6: Strouhal number trend dependent on the Reynolds number for cylinders [25, p. 10]

The vortex-shedding frequency f is dependent on the Reynolds number. The normalized frequency is called Strouhal number St and can be calculated with equation 2.2. Figure 2.6 shows the range and dependency of the Strouhal number and the Reynolds number. Vortex-shedding appears with a Reynolds number higher than 40. The Strouhal number rises from 0.1 to 0.2 between $40 < Re < 300$ and stays stable at 0.2 for a wide range of Reynolds numbers, until a big jump appears at $Re = 3 - 3.5 \cdot 10^5$. [25, p. 10]

2.6 Porous Discs - Grids of Finite Extension

Axisymmetric grids are adopted to induce a pressure drop, smoothen and attenuate velocity profiles and to break up and homogenize turbulent structures in fluid flows. This is an approach to try to simulate wind turbine wakes in wind tunnel investigations. The near wake flow of two different grids (bi- and monoplane disc) is analysed by Pierella and Sætran [17] at $Re = 8 \cdot 10^4$. Their analysis are including computer simulations and wind tunnel measurements. The measurements are done with particle image velocimetry (PIV) and pitot tubes in an area from zero to $6 D$ downstream from the grids.

The regularly spaced axes of a monoplane grid are intersected contrary to a x-wise spacing of the biplane grid. The porosity σ of a grid is defined as "solid frontal area over total frontal area".

For a better comparison between different disc sizes and speeds, is the non-dimensional velocity used:

$$u^* = \frac{u_\infty - u}{u_0} \quad (2.6)$$

$$u_0 = u_\infty - u_{CL} \quad (2.7)$$

It is defined as difference of free stream velocity u_∞ minus wake center velocity u , divided

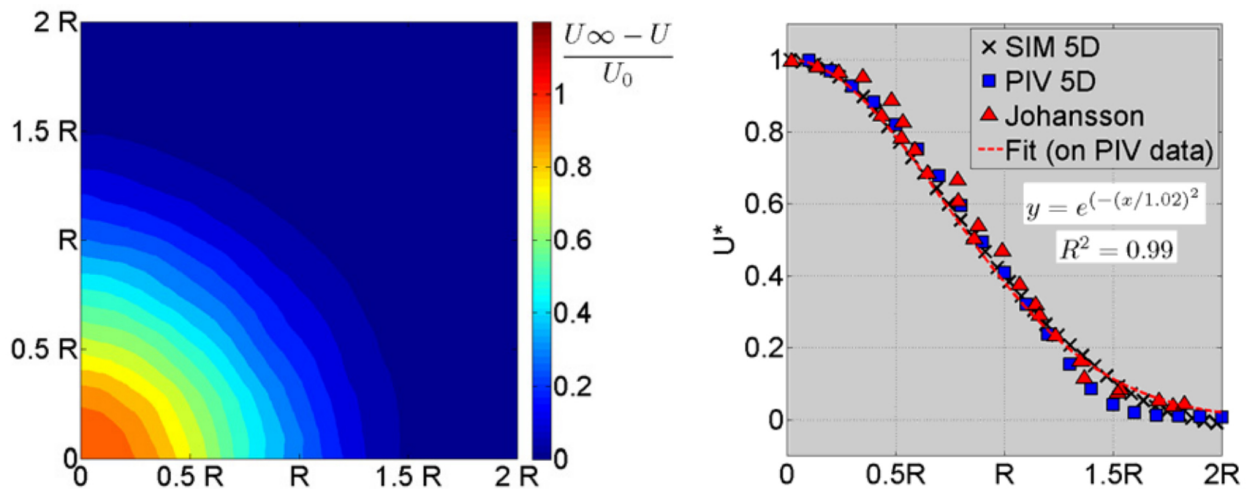


Figure 2.7: Flow behind a porous monoplane disc in $5 D$ distance [17]

by the difference of free stream u_∞ and x-component of wake center velocity u_{CL} .

The determined wake of Pierella and Sætran [17] for a porous monoplane disc is shown in

CHAPTER 2. AERODYNAMIC FUNDAMENTALS

figure 2.7. The simulation of the wake flow behind the porous monoplane disc with Ansys Fluent® software package shows a symmetric shape, whose non-dimensional characteristics is equal to a Gaussian curve. Also the measurement confirm a symmetric flow as in the simulation predicted. Additional information from Pierella, but not content of the paper, states that the drag coefficient C_D for the porous monoplane disc is 0.81. [17]

2.7 Circular Full Disc

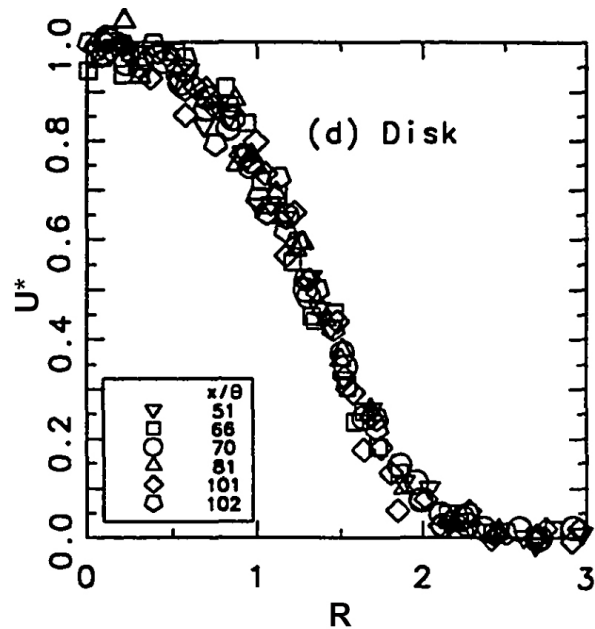


Figure 2.8: Flow behind a circular full disc for different distances [5, p. 58]

Since the early 20th century was a lot of research done on wake flow around a circular flat plate. The wake flow was investigated by Cannon [5] and can be seen in figure 2.8. The drag coefficient C_D has been found to be 1.11 [23, p. 114]. In figure 2.9 can be seen, that the drag coefficient is not constant for all Reynolds numbers. Especially for small Reynolds numbers is the drag coefficient big. For rising Reynolds numbers decreases the drag coefficient until reaching the limit of 1.11 (for all big Reynolds numbers).

Schütz [23] states that turbulence and roughness effects are not having an impact on the flow regime. Additionally he assumes that the high drag bases on a low pressure region behind the plate. The lowest pressure occur immediately behind the plate and increases in the wake flow. This behaviour can be seen for all blunt bodies with defined break-off point and developed wake flows. [23, p. 114] [13, p. 2f]

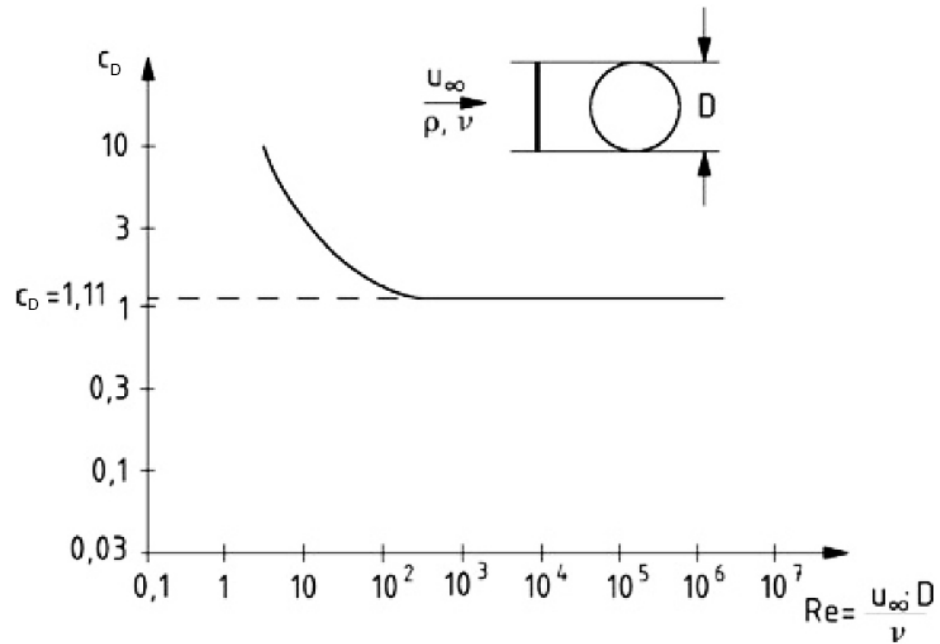


Figure 2.9: Drag coefficients for circular flat plates [23, p. 114]

2.8 Actuator Disc Model

Wind turbines are converting the kinetic energy in the wind by reducing the velocity behind the wind turbine. The aerodynamic consideration of wind turbines can be simplified by using the actuator disc model, which changes the rotor to a thin, circular, permeable disc. This model is good to analyse the overall turbine performance, but it can not replace a design examination of the blades. Kulunk [10, p. 2] notes that the actuator disc model is based on the following edge condition: "...no frictional drag, homogenous, incompressible, steady state fluid flow, constant pressure increment or thrust per unit area over the disk, continuity of velocity through the disk and an infinite number of blades."

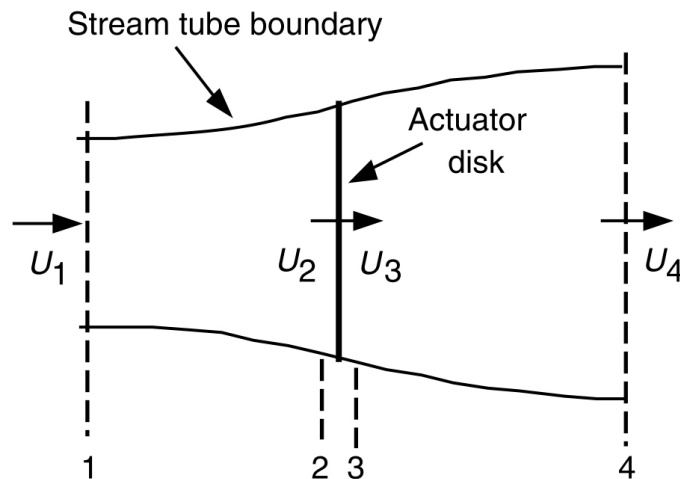


Figure 2.10: Actuator disc model of a wind turbine [11, p. 93]

The described circumstances can be seen in picture 2.10. With regard on the mass conservation law is the control volume smaller in point one than in point two, due to a reduced velocity. The thrust for steady flow is defined as:

$$F_T = \dot{m}(u_1 - u_4) \quad (2.8)$$

In addition can the Bernoulli function be used for the up

$$p_1 + \frac{1}{2}\rho u_1^2 = p_2 + \frac{1}{2}\rho u_2^2 \quad (2.9)$$

CHAPTER 2. AERODYNAMIC FUNDAMENTALS

and downstream tube.

$$p_3 + \frac{1}{2}\rho u_3^2 = p_4 + \frac{1}{2}\rho u_4^2 \quad (2.10)$$

The pressure at the beginning and the end of the control volume are equal ($p_1 = p_4$) as well as the velocities before and after the disc ($u_2 = u_3$). Important for wind turbines is the power output

$$P = \frac{1}{2}\rho A u_1^3 \frac{u_1 - u_2}{u_1} \left(1 - \frac{u_1 - u_2}{u_1}\right)^2 \quad (2.11)$$

and the power coefficient as ratio of rotor power divided by power in the wind.

$$C_p = \frac{P}{\frac{1}{2}\rho u_1^3 A} \quad (2.12)$$

[12, p. 6f] [10, p. 3ff]

2.9 Model Wind Turbine Wake

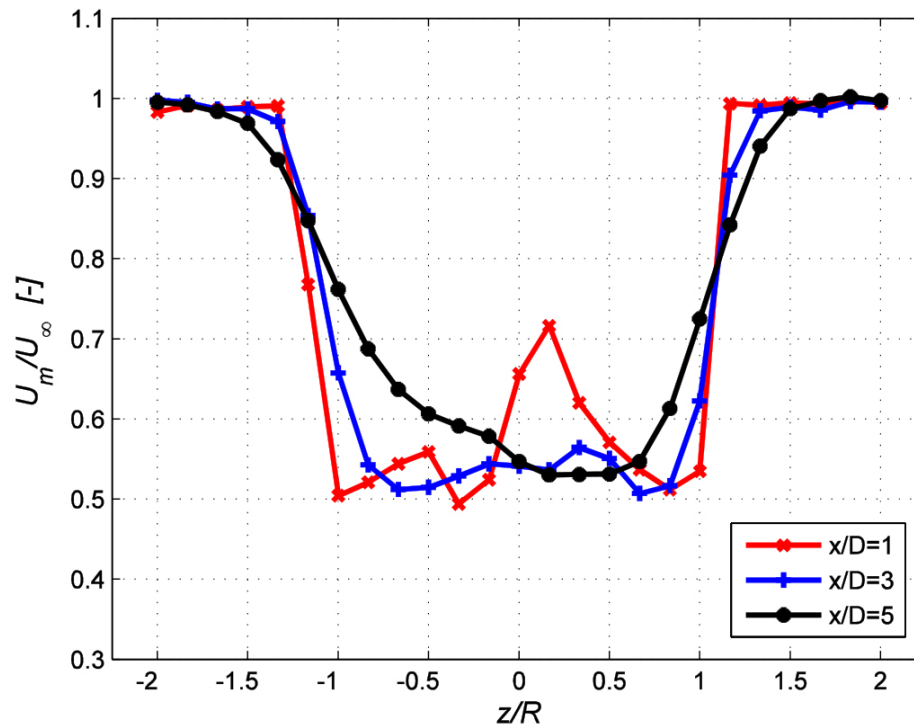


Figure 2.11: Model wind turbine mean wake velocity distribution [1, p. 53]

Bartl [1] measured the mean wake flow distribution U_m/U_∞ behind a model wind turbine, which can be seen in figure 2.11. The measurements were done in a distance of $1 D$, $3 D$ and $5 D$ at 11.5 m/s . The downstream minimum velocities are rising from 5.9 m/s via 6.1 m/s to 6.4 m/s with a growing distance. Additionally the mean wake profiles become broader and the gradients weaker. [1, p. 53 f]

Chapter 3

Measurement Methods

This chapter is reviewing the measurement set-ups and the investigated bodies, that will be used for the experiments described in chapter 4. In the beginning are the wind tunnels and the different technologies to measure forces, pressures and velocities introduced. Some measurement instruments need a calibration before the experiments start. The processes of calibration is presented in the instrument calibration section 3.4. The last section is giving dimensions and properties of the geometrical bodies.

3.1 NTNU Wind Tunnels

For the investigations of this thesis are two wind tunnels from the Energy and Process Engineering Department of NTNU used. They can be seen in figure 3.1. Both tunnels are closed loop wind tunnels of different size.

The smaller wind tunnel has a cross section of 0.50 m x 1.00 m and the maximum wind speed is above 25 m/s. The wind speed can be regulated by a flap valve.

The big one is Norway's biggest wind tunnel, which is also situated at NTNU. It provides a cross section of about 1.90 m x 2.70 m and can generate wind speeds up to 27 m/s. The experimental section is about 11 m long and provides a laminar flow. A traverse with remote control and moving abilities in x, y and z direction is used for static wake measurements.

CHAPTER 3. MEASUREMENT METHODS

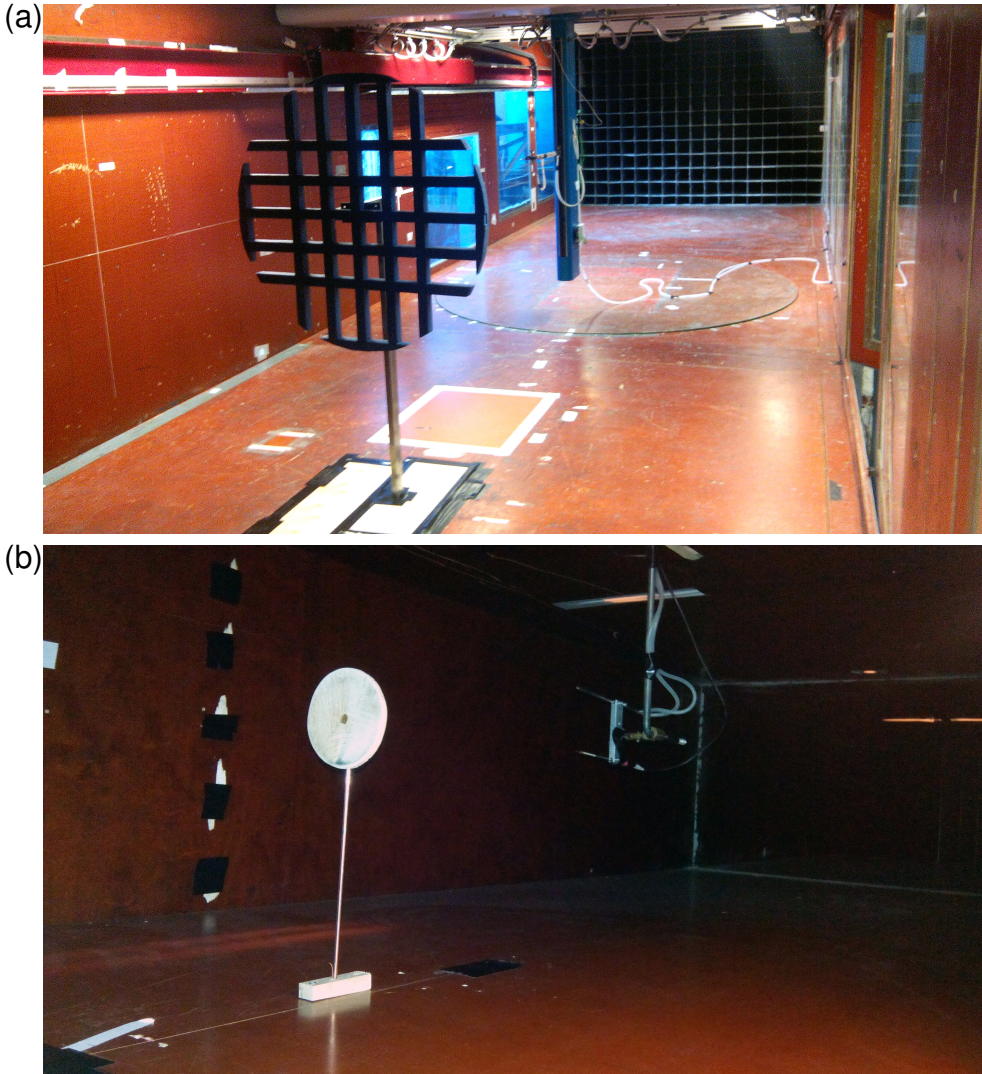


Figure 3.1: (a) Big and (b) small NTNU wind tunnel

3.2 Force Measurement

3.2.1 Strain Gages

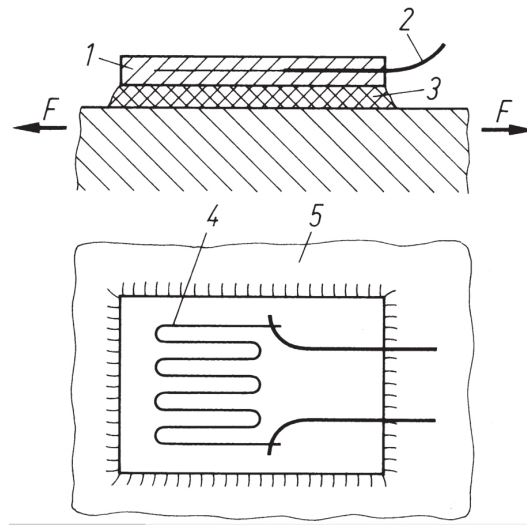


Figure 3.2: Strain gages. 1 carrier material (e.g. polyimide), 2 connecting wire, 3 glue, 4 measuring wire (e.g. constantan), 5 substrate [8, p. W15]

Strain gages will not be used as measurement set-up, but they are part of force plates and pressure transducers. The basic understanding can help to improve the measurements. Strain gages can be used as sensors to measure the alternation of length by using the change of electrical resistance R . They can be used for stretching, pressing, bending and torsion. As seen in figure 3.2 the measuring wire is put into a meander form, so that the electrical resistance change is in a measurable range. Strain gages are usually available with $R = 120, 350$ and 600Ω and are normally limited to a maximal response frequency of 50 Hz. The sensor is attached with glue to the component that is deformed and experiences a length transformation. The resistance is dependent on the specific resistance ρ , the length l and the diameter D :

$$R = \frac{4\rho l}{\pi D^2} \quad (3.1)$$

From that equation is obvious that $R \sim l$. Hence the electrical resistance is rising and dropping with the length of the measuring wire.[8, p. W14f]

3.2.2 Force Plate

Force plates are one of many tools for biomechanists to measure forces and moments. But as described later in chapter 4 are force plates also useful for other applications. Usually strain gages or piezoelectrical crystals are used as sensors. Strain gage platforms have better static skills, but not the same sensitivity and range like platforms with piezoelectric crystals. That means that piezoelectric models should be used for high-frequency applications like vibration analysis.

According to Robertson et al. [20, p. 94], "Most commercial platforms are instrumented to measure in three dimensions - vertical (Z), along the length of the plate (Y), and across the width of the plate (X)." All vectors can be characterized by nine different quantities. First of all by the three orthogonal force vectors F_x , F_y and F_z , plus the positioning of the vectors by using the x, y and z coordinates in relation to a defined reference system for the plate. And finally by the three orthogonal moments M_x , M_y and M_z . [20, p. 92ff]

AMTI - Force Plate

At NTNU's wind tunnel laboratory is the AMTI BP400600-2000 available with a dimension of 400 mm x 600 mm x 82.5 mm. It can handle up to 8900 N vertical (z-direction) and 4450 N side (x- and y-direction) load. Each moments and forces can be measured in three directions. The coordinate system of the platform can be seen in figure 3.3. The force plate needs to be connected to a GEN 5 signal conditioner, which gives an analogue force and momentum signal of ± 10 V out.

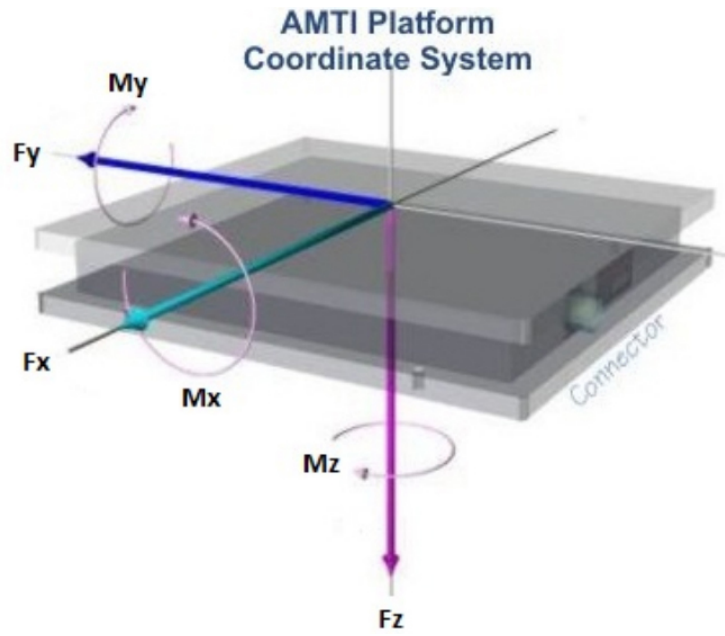


Figure 3.3: Coordinate system of force plate

3.3 Velocity and Pressure Measurements

Measuring the velocity of fluid flows can be done in many ways. The most common methods are based on pressure, optical or thermal scaling. Negative is to mention, that a lot of methods influence the flow parameters by choking or taking energy from the fluid. For example flow meters or the rotameter principle are often inappropriate to measure air flow velocities in a wind tunnel. Contrary the pitot tube and the hot wire anemometry seem to be most promising. They will be introduced in the follow sections.

3.3.1 Pitot Tube

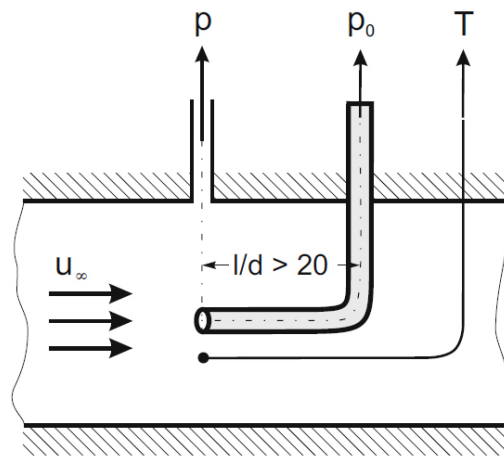


Figure 3.4: Principal structure of a Pitot tube [14, p. 46]

The principal of a velocity measurement with a pitot tube is shown in figure 3.4. This method uses the pressure that occurs due to a retaining effect in front of the tube. The kinetic energy of the fluid is converted to a dynamic pressure, that can be measured e.g. by a pressure differential sensor. The fluid velocity u can be determined by taking the measured dynamic pressure p_{dyn} into account with the density ρ :

$$\frac{\rho}{2} u^2 = p_0 - p = p_{dyn} \quad (3.2)$$

This equation can be converted, to receive an expression of u :

$$u = \sqrt{\frac{2p_{dyn}}{\rho}} \quad (3.3)$$

The density is temperature dependent and can be taken from tables like VDI Wärmesatlas [27]. Pitot tubes have a wide range of applications and are well established. [14, p. 45ff] [8, p. B49]

3.3.2 Contraction

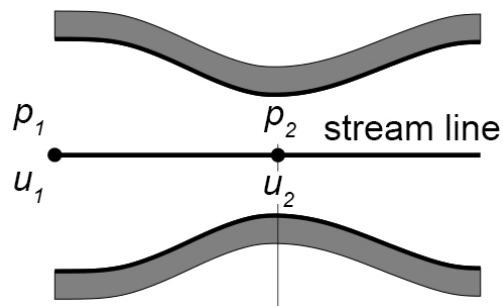


Figure 3.5: Venturi tube (Adapted from [15, p. 80])

A contraction is like half a venturi tube, as seen in figure 3.5. The cross section changes from wide to small, causes a flow acceleration and a reduced pressure at the smallest cross section. This flow change enables to determine the velocity by measuring the pressure difference of the wide and the small cross section. The velocity can be determined with the Bernoulli-equation by measuring the pressure p_1 and p_2

$$\frac{u_1^2 \cdot \rho}{2} + p_1 + \rho \cdot g \cdot z_1 = \frac{u_2^2 \cdot \rho}{2} + p_2 + \rho \cdot g \cdot z_2 = const. \quad (3.4)$$

and the continuity equation.

$$A_1 \cdot \rho \cdot u_1 = A_2 \cdot \rho \cdot u_2 \quad (3.5)$$

The continuity equation is shifted to

$$u_1 = \left(\frac{A_2}{A_1}\right)^2 \cdot u_2 \quad (3.6)$$

and introduced in the simplified and converted Bernoulli equation. It is assumed that $z_1 = z_2$:

$$u_2 = \sqrt{\frac{2(p_1 - p_2)}{\rho \cdot \left[\left(\frac{A_2}{A_1} \right)^2 - 1 \right]}} \quad (3.7)$$

With the knowledge of the pressure difference $p_1 - p_2$ and the cross section proportion $\left(\frac{A_2}{A_1} \right)^2$ can the wind tunnel inlet velocity u_2 be determined. [15, p. 79]

3.3.3 Pressure Transducers

Pitot tubes and the contraction need to be connected to pressure transducers. The connection is facilitated by plastic hoses, which transmits the pressure level. The transducers are basically converting the pressure into an electrical signal. The hoses should be held as short as possible, to ensure that the response frequency of the system is high enough. Nitsche and Brunn [14] divide pressure transducers in absolute, sealed and differential pressure systems. Most used are differential sensors, which will be used for this thesis. Usually, the pressure is affecting an elastical membrane, which is e.g. connected to strain gages, piezo electric sensors, or inductive or capacitive sensors. Mostly is the signal amplified to a signal between -10 V and +10 V by internal electronics. Otherwise an external amplifier is used. [14, p. 24ff]

3.3.4 Hot Wire Anemometry

Hot wire anemometers basically consist of a thin wire that is fixed to the end of a fork like instrument. Most common is the Constant-Temperature-Anemometry (CTA). The set-up in a bridge circuit is shown in figure 3.6. The hot wire is heated up to a temperature above the flow temperature. Due to the heat loss of the wire is the electrical voltage linked to the speed. This effect uses the temperature-resistance dependency of the hot wire. The bridge circuit is needed to regulate the voltage by adapting the resistance R_0 . The voltage U_B can be linked to the speed after a calibration e.g. with a pitot tube. The biggest advantage is a high response frequency, which makes the use interesting for high turbulent flows. Important is the knowledge about the flow direction, otherwise will the

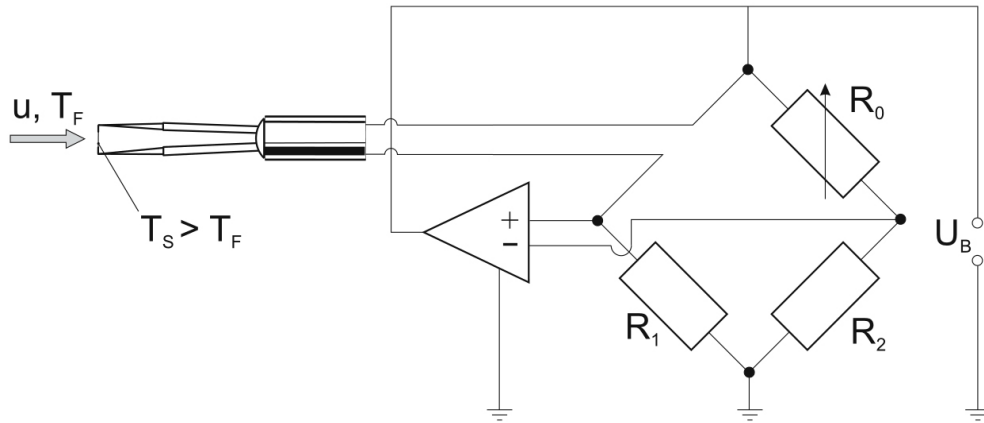


Figure 3.6: Principal circuit of a constant temperature hot wire anemometer [14, p. 49]

data vary from the real flow velocity. [14, p. 49 ff]

3.4 Instrument Calibrations

3.4.1 Pitot Tube and Contraction

The pitot tube and contraction set-up needs to be calibrated before hand, to interpret the electrical signals given by the pressure transducers. Therefore is an u-tube manometer like instrument used. It is filled with alcohol and has a scale. The angel of the scale can be adapted to change the measure range. Important is a nullification and an adjustment parallel to the ground. The manometer is additionally connected to the hoses, that connect the pitot tube or the contraction and the pressure transducer.

With the level of alcohol h , the gravity acceleration g , the density of alcohol ($\rho = 810 \text{ kg/m}^3$) and the quotient of the angel k , can the pressure difference be calculated:

$$\Delta p = h \cdot g \cdot \rho \cdot k \quad (3.8)$$

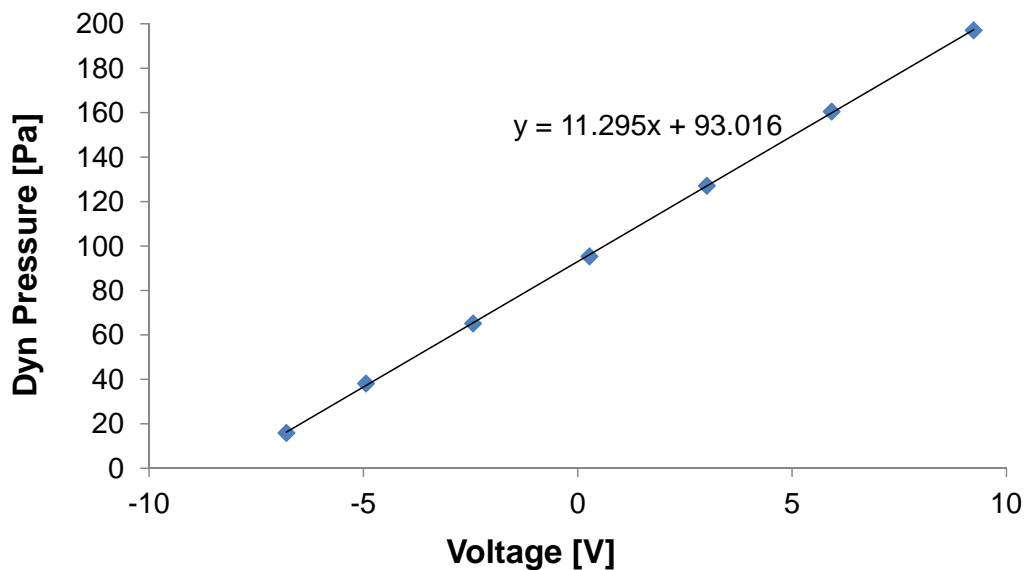


Figure 3.7: Pitot tube calibration curve, with best-fit line and equation

The pressure and the electrical signal can be plotted in a diagram. An example can be seen in figure 3.7. The equation describing the best-fit line is used for the experimental measurements.

3.4.2 Hot Wire Anemometer

Also the hot wire anemometer needs a calibration, to determine the operating resistance R_{op} and the response frequency. The used hot wire anemometer has a resistance $R_{w,c}$ of 5.7Ω . Before starting the experiments need the total resistance R_{tot} and the anemometer resistance R_{an} to be determined. With these quantities and the following two equations can the operation resistance be identified.

$$F = \frac{R_{an}}{R_{tot}} \quad (3.9)$$

$$R_{op} = (1.5 \cdot R_{w,c} + R_{tot} - R_{w,c}) \cdot F \quad (3.10)$$

The over heat factor of 1.5 is an approximate result of the heat transfer equation

$$R_{w,h} = R_{w,c}(1 + \alpha(T_w - T_{ref})) \quad (3.11)$$

Where T_w is about $300 \text{ }^\circ\text{C}$ and T_{ref} about $20 \text{ }^\circ\text{C}$.

The response frequency can be determined, by giving an electrical step signal to the hot wire. Out of the length of a whole response can the response frequency f_{res} be calculated with

$$f_{res} = \frac{1}{1.3 \cdot t} \quad (3.12)$$

The operating resistances and the response frequencies are expected to be around 10Ω and $7000 - 12000 \text{ Hz}$.

A pitot tube is as reference needed, to get the velocity calibration curve. The best-fit lines are in that case not linear, but a graph of a higher degree polynomial (usually three or five). An example of a best-fit line can be seen in figure 3.8.

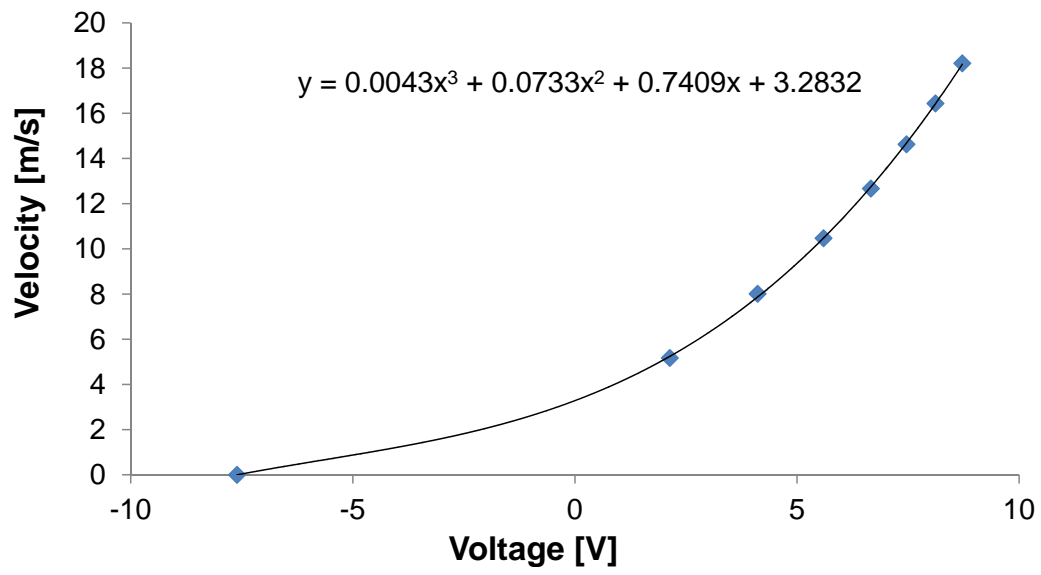


Figure 3.8: Hot wire anemometer calibration curve, with best-fit line and equation

3.5 Cylinder, Porous Monoplane and Circular Full Disc Design

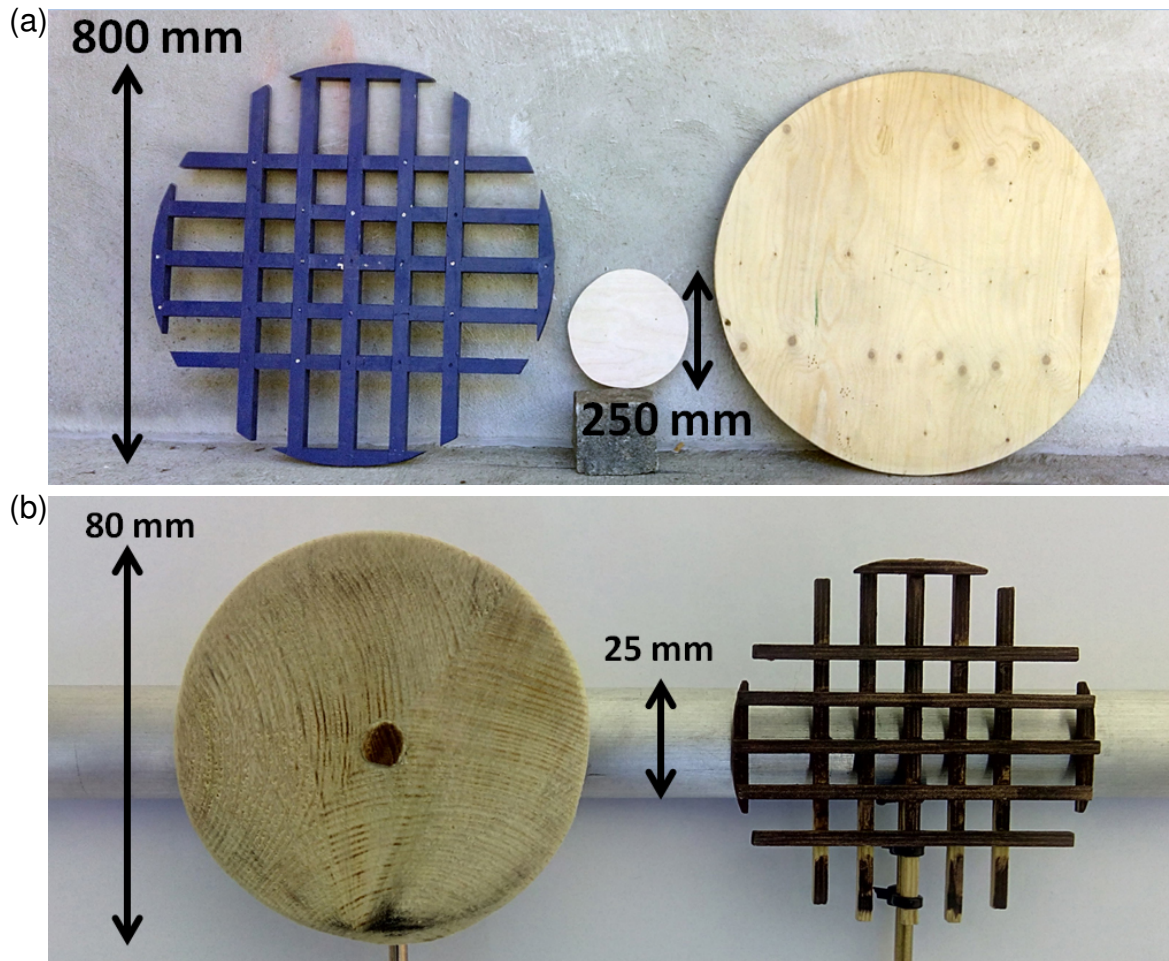


Figure 3.9: Investigated bodies: (a) 800 mm and 250 mm discs for the big wind tunnel. (b) 80 mm discs and 25 mm cylinder for the small wind tunnel

In the following experiments will several geometrical bodies be investigated. The bodies are a cylinder, two porous discs and circular full discs, as seen in figure 3.9. For experiments in the big wind tunnel will the bodies in the upper picture (a) be used. Downscaled for experiments in the small wind tunnel are the discs and the cylinder in the bottom picture (b) of figure 3.9 used.

The Cylinder is made of aluminium, with a smooth surface. It is about 1 m long and has a diameter of 25 mm. The porous monoplane and the biggest circular full discs have a diameter of 800 mm. Additionally are smaller circular full discs with a diameter of 250 mm

CHAPTER 3. MEASUREMENT METHODS

and 80 mm and a porous biplane disc with a diameter of 80 mm used. All the discs are made of wood.

As porous discs are the monoplane and the biplane disc from Pierella and Sætran [17] used. Monoplane means that the mesh bars are in one level and not attached on each other like a biplane design. Both the monoplane and the biplane discs have a porosity of $\sigma = 55\%$. All the discs are centrally attached to stands. The big stand is 1 m and the small stand 0.23 m long.

Chapter 4

Experimental Results

This chapter contains the main work of this thesis. Aerodynamical and mechanical investigations will be done on a cylinder, porous discs and circular full discs. Before gives section 4.1 an introduction on investigated quantities and presents theoretical estimations. The goals, set-up's as well as the data and interpretation will be part of sections 4.2, 4.3 and 4.4, connected to each experiment. Finally is an error analysis and a comparison of the mean wake velocities with a model wind turbine included.

4.1 Preparatory Work

4.1.1 Aerodynamic Forces

From special interest are the drag forces of all investigated bodies. The drag forces are generated by the aerodynamical resistance. The focus of this section is set on the appearing drag forces, the drag coefficients and the Reynolds Numbers. The estimations of the quantities in dependency of the wind velocity are presented in table 4.1. The drag force is determined with equation 2.3 and the Reynolds number with euqation 2.1. The density and the kinematic viscosity of air at 20 °C are taken from Verein Deutscher Ingenieure VDI [27] Wärmeatlas ($\rho = 1.1885 \text{ kg/m}^3$ and $\nu = 153.7 \cdot 10^{-7} \text{ m}^2/\text{s}$). A is the surface that faces the wind.

As the drag coefficient is proportional to the surface and the velocity, has the circular full

Table 4.1: Estimated aerodynamic dimensions

	Cylinder	Circular full disc	Porous monoplane Disc
D [m]	0.025	0.8	0.8
A [m ²]	0.025	0.503	0.503
C_D [-]	1.2	1.11	0.81
F_D (5 m/s) [N]	0.446	8.289	6.049
F_D (10 m/s) [N]	1.783	33.156	24.195
F_D (15 m/s) [N]	4.011	74.601	54.439
Re (5 m/s) [-]	8159.3	261096.6	261096.6
Re (10 m/s) [-]	16318.5	522193.2	522193.2
Re (15m/s) [-]	24477.8	783289.8	783289.8

disc the highest drag forces. The differences between the porous monoplane and the circular full drag disc is only the drag coefficient. The Reynolds numbers of the discs are equal, due to the same diameters. Contrary to the discs are the forces for the cylinder small. Also the Reynolds number is considerably smaller.

4.1.2 Cylinder Vortex Shedding

For the frequency analysis in section 4.4 is an estimation of the cylinder vortex frequency needed. This can be done with the Strouhal equation 2.2. Additionally is known from figure 2.6, that the Strouhal number is $St= 0.2$ for a wide range of Reynolds numbers.

$$f = \frac{St \cdot U}{D} = \frac{0.2 \cdot 15 \text{ m/s}}{0.025 \text{ m}} = 120.0\text{Hz} \quad (4.1)$$

The vortex frequencies for different wind velocities can be seen in table 4.2. These fre-

Table 4.2: Estimated vortex frequencies

	Frequency [Hz]
f (5 m/s)	40
f (10 m/s)	80
f (15 m/s)	120

quencies can serve for estimating sampling frequencies. The range of the vortex frequency for velocities between 10 m/s and 15 m/s can be estimated as 80 to 120 Hz.

4.2 Static Cylinder Measurement

4.2.1 Goal of Experiment

This experiment is done to measure a flow behind a smooth metal cylinder. The mean wake velocity allocation will be compared to suitable literature. Furthermore the drag measurement by wake method from section 2.3 will be validated. The mean wake flow will be determined by screening with a pitot tube. The literature known drag coefficient needs finally be compared to the calculated drag coefficient determined by the wake survey method.

4.2.2 Experimental Set-up

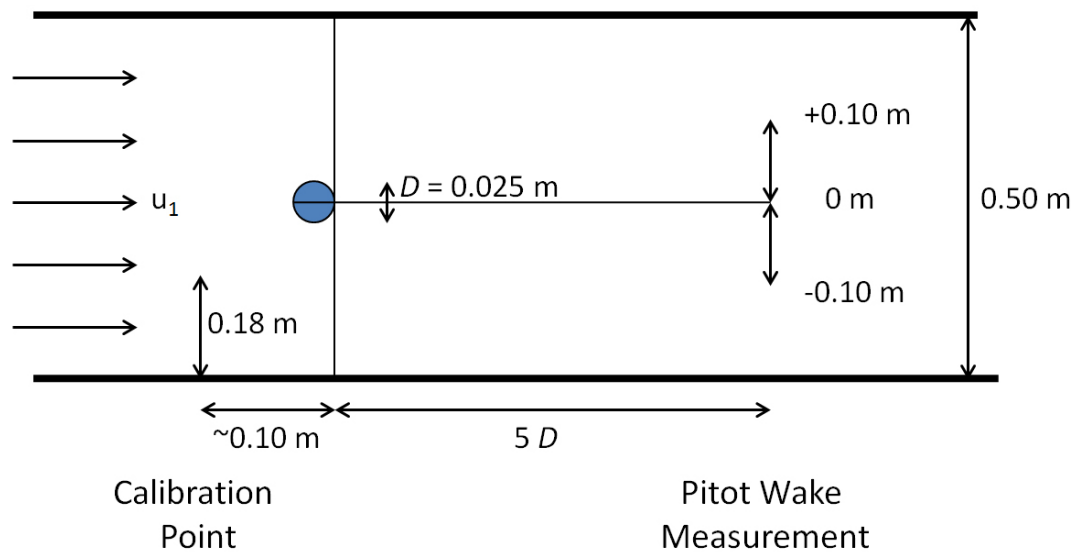


Figure 4.1: Wind tunnel arrangement for cylinder wake measurement

The cylinder measurements are performed in the small wind tunnel. The wind tunnel arrangement can be seen in figure 4.1. The cylinder is fixed on both sides in a horizontal position at about the middle of the wind tunnel. A pitot tube is used to raster the wake flow behind the cylinder in $5D$ diameter distance from the cylinder. Rastering behind the wake is done in a vertical way starting at +100 mm above the center of the cylinder and ending at -100 mm. The calibration curve is taken beforehand, 180 mm above the ground and

about 100 mm in front of the cylinder, to have a laminar inlet flow.

4.2.3 Results

Wake Velocities

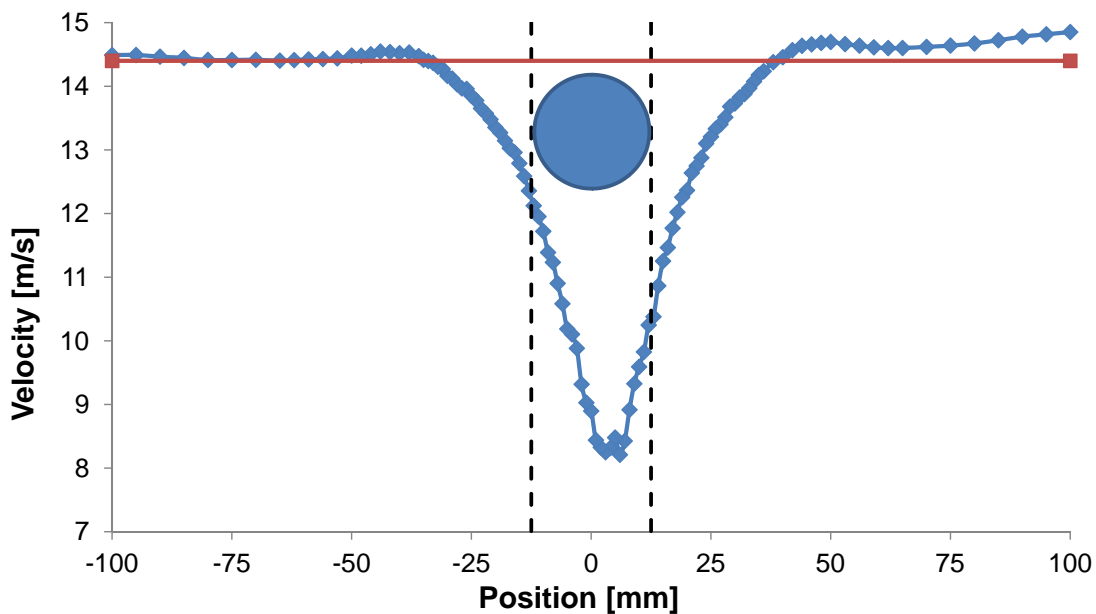


Figure 4.2: Mean velocity allocation behind a cylinder at $5 D$ distance (blue) and the asymptotic velocity (red)

The acquired voltage signals are converted with the recorded calibration curves. The calculated dynamic pressure and velocity in the wake are presented in table A.1 and A.2. The same data can be seen in figure 4.2, which shows the flow speed over the wake position (blue graph). The red line states the asymptotic wind speed of 14.4 m/s. It can be seen that the graph is approximately axis symmetric, by an axis in the center of the cylinder. At the position directly behind the center of the cylinder is the least velocity of about 8 m/s located. The velocity is rising towards the outside of the direct wake. Peaks can be recognized at each side at -44 mm and 50 mm with about 14.6 m/s, before the wind speed normalizes towards the edges of the diagram. The Reynolds Number is about 23 500. The graph in figure 4.2 shows a distinctive symmetric wake flow of cylinders. A Reynolds number of 23 500 implies a completely turbulent wake flow with vortex streets. This can

CHAPTER 4. EXPERIMENTAL RESULTS

not be seen in the measurements, due to the fact that they are 10 s time-averaged. To see vortices in the wake, a measurement set-up is needed that is fast reacting, not time-averaging and continuously measuring.

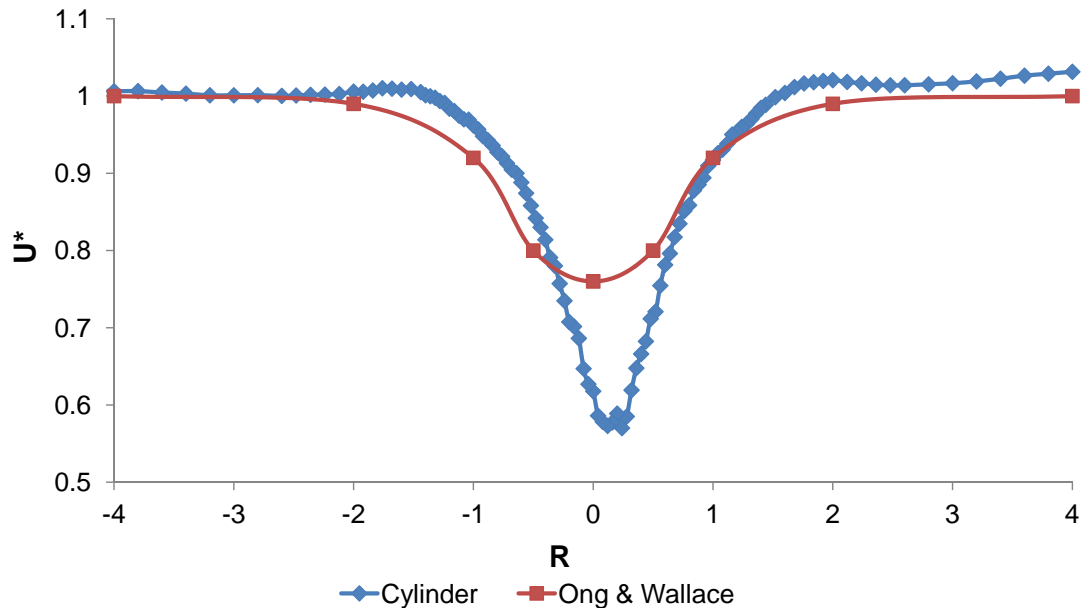


Figure 4.3: Non-dimensional mean velocity allocation for the cylinder compared to Ong and Wallace [16]

The measured wake flow of figure 4.3 does not fit totally with the curves given by Ong and Wallace [16]. The dimensionless velocity U^* is defined as

$$U^* = \frac{U_{mean}}{U_{inlet}}$$

As predicted is the lowest velocity directly behind the cylinder. However is the lowest point for the measured curve lower than the Ong and Wallace [16] curve. The gradients on the outside seem to have a similar gain. The peaks left and right of the bottom point can be a result of the acceleration due to the separation around the cylinder.

Drag Coefficient

The drag coefficient is calculated with a Matlab program, that contains the drag measurement by wake method. It contains equation 2.4 for the drag force F_D and equation 2.5 for the drag coefficient C_D . The calculated drag coefficient is measured to be 0.9, which is in the same dimension like the 1.2 that Sumer and Fredsoe [25] specified. The big difference between the measured and the literature value can not be explained, but it was found, that the inlet velocity in front of the cylinder has a strong influence on the determined drag coefficient. In a sensitivity analysis was identified, that a difference of 0.1 m/s has an impact of more than 3 % on the result. Maybe a velocity measurement with a pitot tube in front of the cylinder would bring better results for the drag coefficient.

4.2.4 Conclusions

The results of this experiment are not totally conform with the literature prediction. But the measurement with a pitot tube seems to be applicable for mean wake flow allocation measurements. The accuracy and response of the measurement set-up seem to be convenient for averaged mean velocity measurements in turbulent air flows behind bodies. Furthermore the results show, that the measurement by wake method is really sensitive. Special attention should be paid to measure accurate inlet velocities, since the drag coefficient determination is strongly influenced by this velocity. For the analysis of this experiment was the asymptotic velocity taken. Pitot tube measurements in the upstream could possibly bring better results.

The next step is the application of the wake flow allocation measurements and the survey by wake method for more complex bodies. Therefore are the next experiments done with a porous monoplane and circular full disc.

4.3 Static Porous Monoplane and Circular Full Disc Measurements

4.3.1 Goal of Experiment

In this experiment the drag coefficient of a porous monoplane and a circular full disc will be determined with two different methods. The drag measurement by wake method as well as the force survey method will be used. Therefore the wake flow of the discs will be measured in horizontal direction. Also the vertical wake flow will be measured, to test the equal allocation of the wake flow. Additionally the drag coefficient can be calculated by using the measured drag force from the force platform installed underneath the wind tunnel. Finally, the wake flow allocation and the drag coefficients of both methods will be compared with literature found drag coefficients.

4.3.2 Experimental Set-up

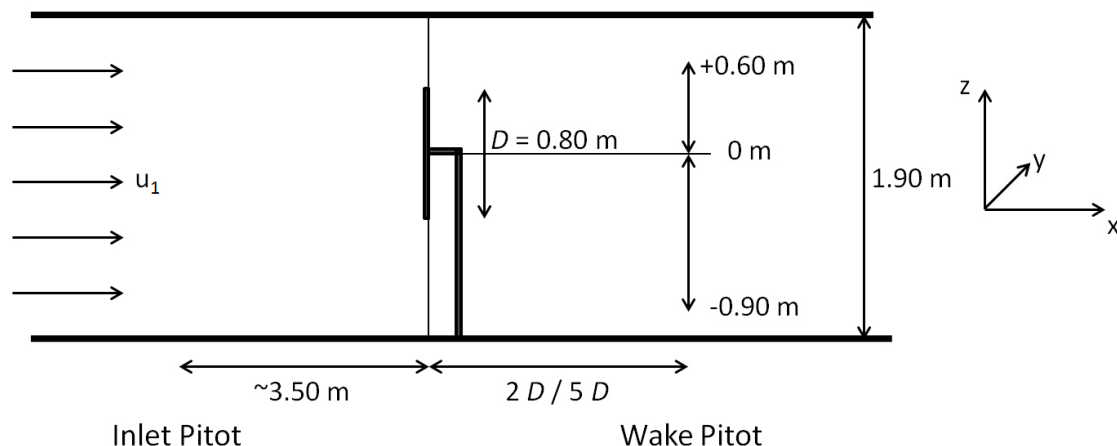


Figure 4.4: Wind tunnel arrangement for full drag disc and porous monoplane disc wake measurement

Both discs need to be fixed on a stand, which is mounted on the force plate in the big wind tunnel. The force plate is located and fixed under the ground of the wind tunnel. Figure 4.4 shows the arrangement in the wind tunnel and the most important dimensions. The discs are mounted approximately in the center of the tunnel. The height of the

CHAPTER 4. EXPERIMENTAL RESULTS

disc center is 925 mm above the wind tunnel ground and the diameter of the discs are $D = 800$ mm. The distances to the left wall is 1308 mm and to the right wall 1415 mm. The horizontal and vertical centric wake is measured in $5 D$ distance behind both discs. The first measurements are done with an inlet pitot tube, for the inlet velocity. It is mounted about 3.50 m in front of the disc. Later is a measurement set-up with the contraction used. The wake pitot tube is fixed on a traverse, which is movable and can be positioned remotely. The pitot tubes are calibrated, before starting the experiments. Therefore the wake pitot tube is arranged 1.60 m in front, but between disc and wall, to have a free downstream behind the tube. The sample time is raised to 30 s, to have more stable measurements.

4.3.3 Results

Wake Velocities

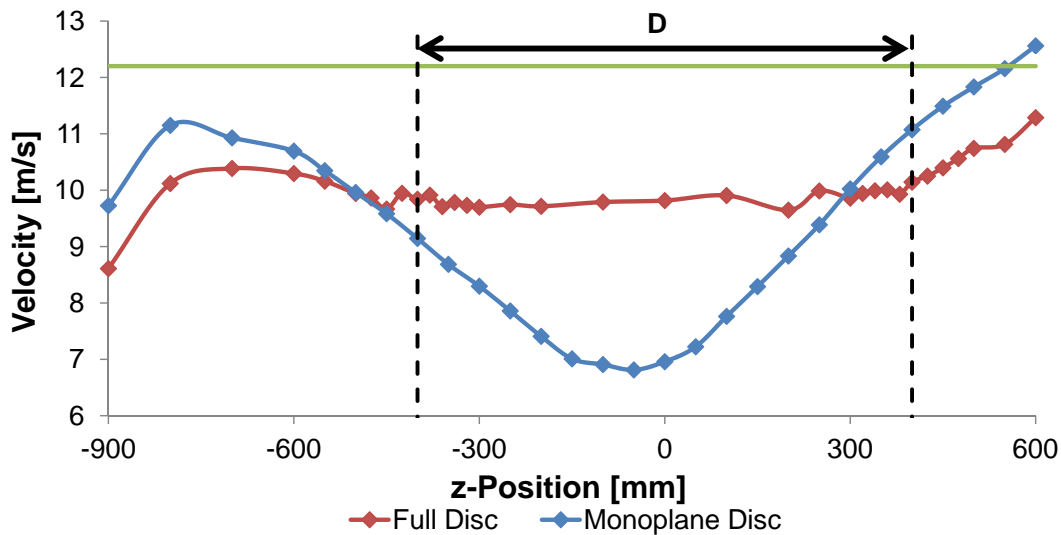


Figure 4.5: Vertical velocity allocation behind the porous monoplane (blue) and the circular full (red) disc at $5 D$ distance and the inlet velocity (green)

The voltage signals from the pitot tubes, the contraction system and the force plate are converted to their equivalent pressures, velocities and forces. The processed data is at-

CHAPTER 4. EXPERIMENTAL RESULTS

tached in table A.3 for the horizontal and table A.4 for the vertical measurements. The velocities in the wake flow are illustrated over the vertical and horizontal position in figure 4.5 and 4.6.

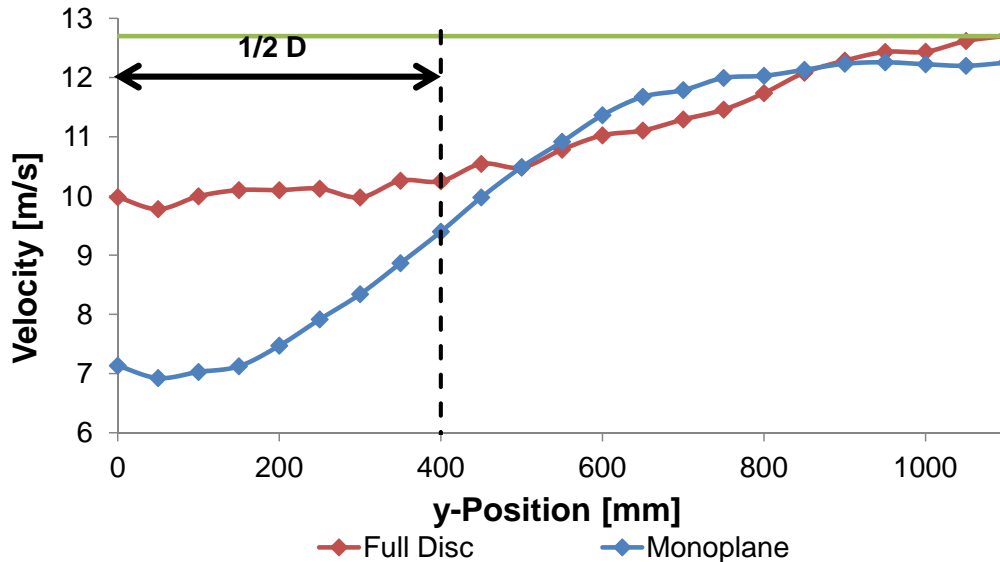


Figure 4.6: Horizontal velocity allocation behind the porous monoplane (blue) and the circular full red) disc at $5 D$ distance and the inlet velocity (green)

The data analysis is done for the graphs seen in figure 4.6. The data of figure 4.5 was not accurate enough and should only show the axis symmetry around the center of the discs, as well as a similar development of the wake flow in vertical direction. The edges of the vertical measured field show a reduced speed on the left and a bigger speed on the right side. The reduced speed on the left side is most likely effected by the friction of the wind tunnel floor. On the other hand might the higher velocity on the right side be a result of the wind tunnel traverse, which reduces the flow area on top by about 200 mm. The constrained flow is probably accelerated and causes a higher velocity than the inlet velocity and might shift the wake flow allocation more to the left side.

The graph for the monoplane disc in figure 4.6 has the lowest wake velocity of about 7 m/s, behind the center of the disc. The trend is similar to the cylinder wake flow of section

CHAPTER 4. EXPERIMENTAL RESULTS

4.2. Which means that the flow velocity is rising with a growing distance from the center. The stream outside the disc diameter is with about 12 - 13 m/s faster than the inlet flow, which is 11.4 m/s. This is probably the influence of the reduced flow field cross section. As seen in figure 4.7 the identified curve for the monoplane disc does fit with the curve determined by Pierella and Sætran [17]. The dimensionless velocity U^* is defined as:

$$U^* = \frac{U_{inlet} - U_{mean}}{U_{inlet} - U_{minimum}} \quad (4.2)$$

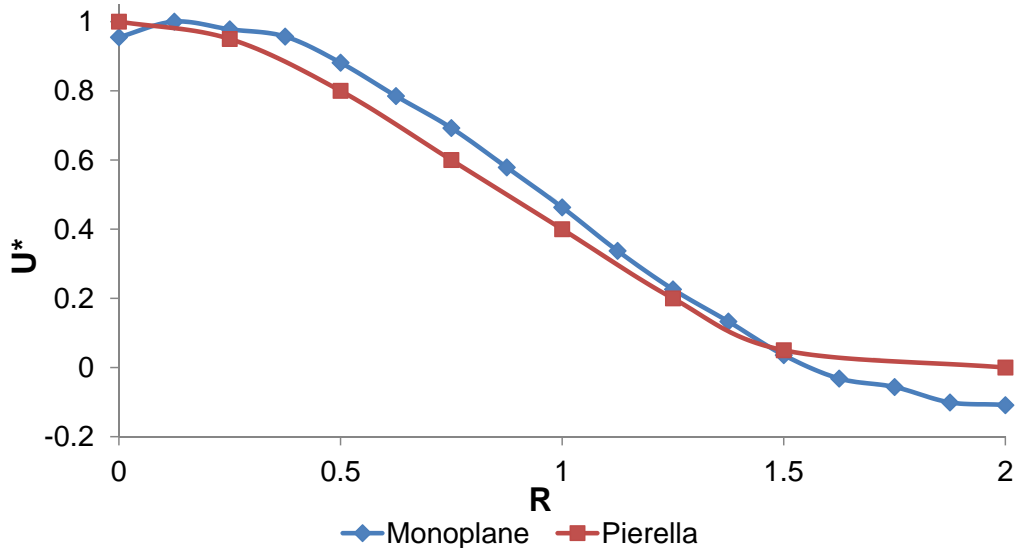


Figure 4.7: Comparison porous monoplane disc measurements with Pierella and Sætran [17]

In contrast the velocity directly behind the circular full disc is about 10 m/s. It does not show a developed wake flow, with a distinctive low point in the center, like the cylinder and the porous monoplane disc. The velocity is rising outside of the direct disc wake and the highest point is above the inlet flow speed, at the right edge of the diagram in figure 4.6. In figure 4.8 the dimensionless results of the full disc measurements can be compared with the measurements done by Cannon [5]. The beginning is at least in the same range but after 1.5 R is the measured curve clearly lower than the literature curve. One of the

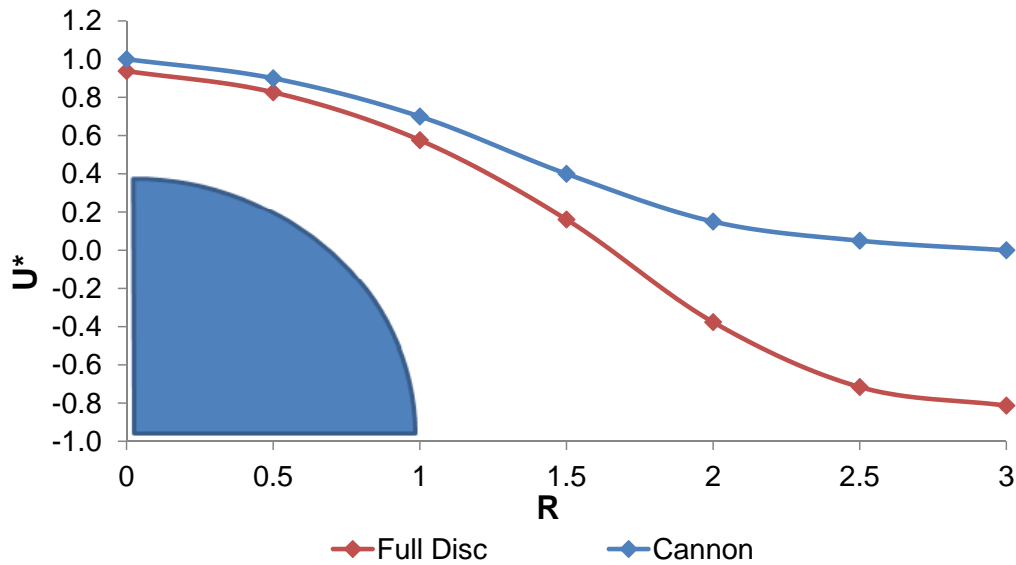


Figure 4.8: Comparison of full disc measurements with measurements of Cannon [5]

differences is the measurement distance behind the disc. Most of the measurements done by Cannon [5] are done in bigger distances. A possibility can be, that the wake is strong turbulent and not yet fully developed. Also problems with the pitot tubes can occur. Pitot tubes can measure in turbulent flows, but it might have problems, if the vortices induce side and back flows. Nitsche and Brunn [14, p. 16] state, that the angle of incidence needs to be smaller than 10° to 40° , depending on the pitot tube design. Also a big blockage can change the result massively on the outsides of the flow. The velocity is higher and causes negative dimensionless velocities, as seen in figure 4.8.

Drag Coefficients

The next step is the determination of the drag coefficients with the force survey and the measurement by wake method. For the measurement by wake method is a Matlab script written, which uses the values that are shown in figure 4.6. First is a function with an interpolation command created. Afterwards is a grid generated, which contains the x and y positions, but only contains the first quadrant of the Cartesian coordinate system. The interpolated equation is circular rotated around the origin and gives the velocity profile for

CHAPTER 4. EXPERIMENTAL RESULTS

1/4 th of the disc. Finally is an area integration command used and introduced in the drag force equation 2.4 and later in the drag coefficient equation 2.5. The rotated wake flows for the porous monoplane and circular full discs are shown in figure 4.9. The colours mark the different velocities. In both cases can be seen that the centers have the lowest velocities.

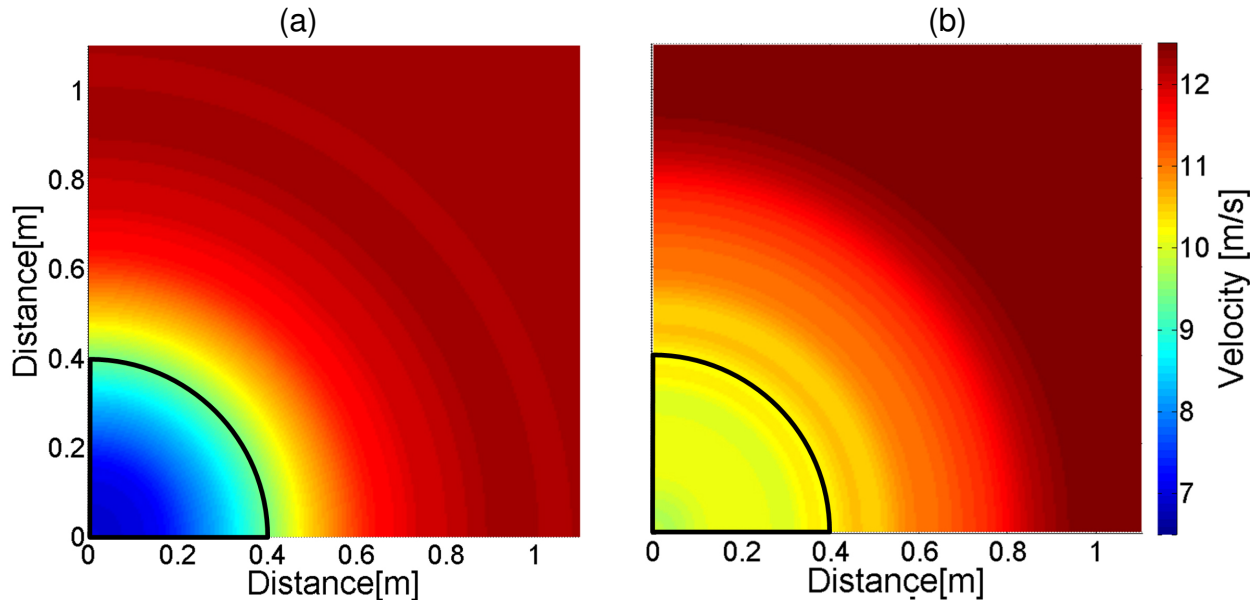


Figure 4.9: Velocity allocation of rotational wake behind (a) a porous monoplane disc and (b) a circular full disc

Table 4.3: Comparison of determined drag coefficients

	F_D [N]	u_1 [m/s]	$C_{D,force}$ [-]	$C_{D,wake}$ [-]	$C_{D,ref}$ [-]
Porous monoplane disc	29.6	11.5	0.77	0.82	0.81
Circular full disc ($D = 0.80$ m)	67.4	11.4	1.78	1.18	1.11
Circular full disc ($D = 0.25$ m)	4.3	11.5	1.15	-	1.11

Table 4.3 gives the determined drag coefficients and the literature values. With a force of about 30 N and an inlet velocity of 11.5 m/s is the drag coefficient 0.77 for the porous monoplane disc. The drag coefficient determined with the measurement by wake method gives 0.82. The identified values fit good with the reference of 0.81 from Pierella and Sætran [17].

The literature predicts a drag coefficient of 1.11 for the circular full disc. But contrary the force survey results in a higher value of 1.78. The measurement by wake method gives

CHAPTER 4. EXPERIMENTAL RESULTS

a C_D of 1.18, which is a good approach to the literature value of 1.11. Some screening experiments were done to be sure all parameters are correctly measured:

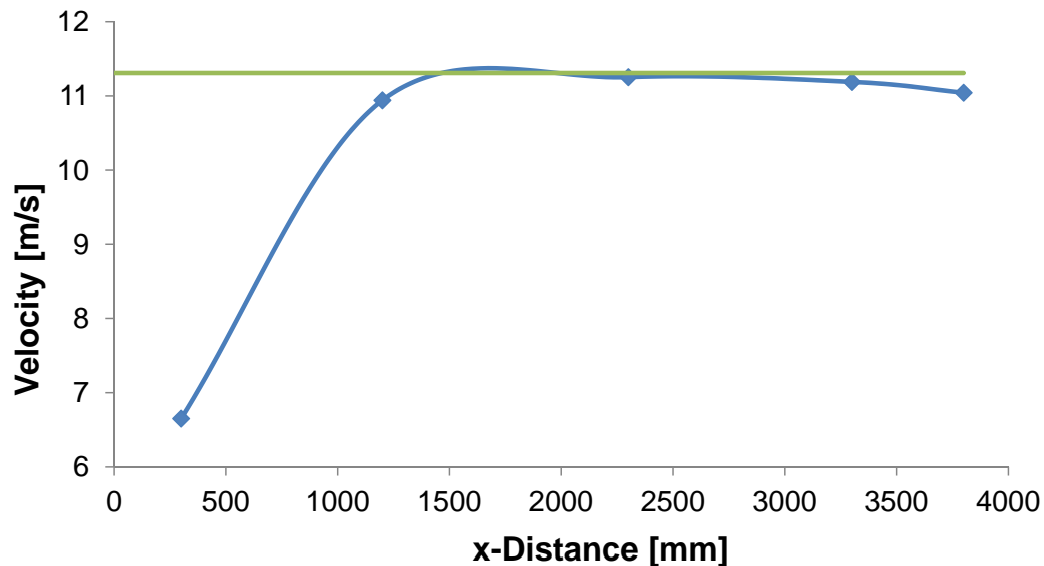


Figure 4.10: Velocity allocation (blue) in front of the full drag disc center with growing distance (Contraction inlet velocity is green)

1. Pretty important is the inlet velocity. Small deviation can have a big impact on the result. The velocity allocation in front of the circular full disc center can be seen in figure 4.10. The velocity is massively influenced by the disc until 1.3 m ahead of the disc. Further away is the velocity almost constant and only varying with about 0.2 m/s. The difference between the contraction measured velocity and the velocity in front of the disc is marginal and can be influenced by the blockage of the drag disc.
2. For a better understand was also the flow 30 cm in front and aside of the disc investigated. The result can be seen in figure 4.11. The flow in front has its lowest velocity of about 6 m/s in the center of the disc and raises to 9.4 m/s at the edge of the disc. The free room between the front and the aside line is left out, due to inconsistent measurements. Probably are turbulences next to the disc affecting the pitot tube recorded values. The aside line rises pretty fast from 5 m/s in 4 cm disc distance to about 13 m/s in 10 cm disc distance. The rest of the line stays stable

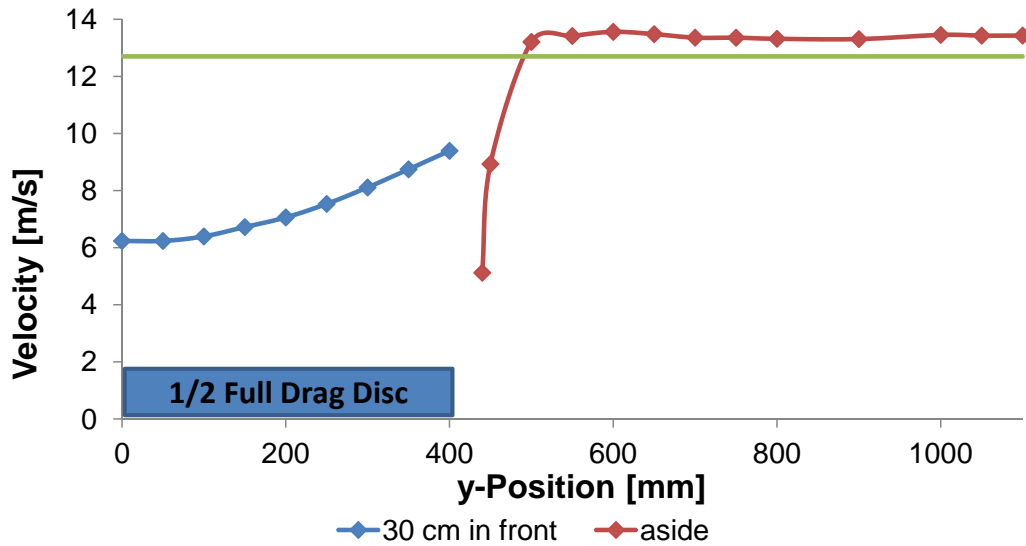


Figure 4.11: Velocity allocation 30 cm in front (blue) and directly aside (red) the full drag disc

at about the 13 m/s. The reduced velocity next to and in front of the disc can be the result of the blockage, turbulences and the surface friction of the disc. The higher velocity in more than 10 cm distance aside the disc is also caused by the blockage, which is generated by the reduced cross section of the wind tunnel. The flow around the disc is accelerated.

3. One problem of the full drag disc, can be the blockage effect. The total cross section of the wind tunnel is 5.13 m^2 . That implies a blockage of about 10 % with a disc surface of 0.503 m^2 . The Engineering Sciences Data Unit [7] gives an equation to eliminate the blockage influence:

$$\frac{F_c}{F_m} = 1 - \frac{k \cdot S}{A} \quad (4.3)$$

Converted and quantities introduced is the following equation given:

$$F_c = \left(1 - \frac{k \cdot S}{A}\right) \cdot F_m = \left(1 - \frac{2.84 \cdot 0.503\text{m}}{5.13\text{m}}\right) \cdot 1.78 = 1.28$$

Also the resulting drag coefficient of 1.28 is higher than expected and not a satisfying

match.

To validate the force survey method with a lower influence of the blockage effect, is a smaller circular full disc with a radius of 0.25 m tested. The influence of the support structure is calculated and taken-off. The results are presented in table 4.3. The drag coefficient of 1.15 generated by the small disc matches good with the 1.11 given by the literature. This states that the force by wake survey works properly with the measurement set-up, but that the impact of the blockage effect might be underestimated.

4.3.4 Conclusions

These experiments have shown, that the measurement by force and by wake survey method work properly. As in the previous experiment in section 4.2 is the influence of the inlet velocity big on the measurement by wake method. Additionally should circular full disc measurements be done with smaller discs, to reduce the blockage effect, which seems to be easily underestimated for the measurement by force survey method. The measurement set-up suits the static measurements. Only the turbulences behind the circular disc might be better measured with sensors that can diagnose the direction of the flow or are flow direction independent. Additionally could a measurement distance of more than $5 D$ give a better developed mean wake flow curve.

4.4 Vortex shedding in the Wake of Cylinder, Porous Mono-plane and Circular Full Disc

4.4.1 Goal of Experiment

In this experiment will the velocities in the wake flows of a cylinder, a porous biplane disc and a circular full disc be recorded as time series. The goal is to perform a vortex shedding analysis. The cylinder vortices are well known and the vortex frequencies can be compared with calculated values. Afterwards the continuous recorded wake flows of the porous biplane and the circular full disc will undergo a frequency analysis.

4.4.2 Experimental Set-up

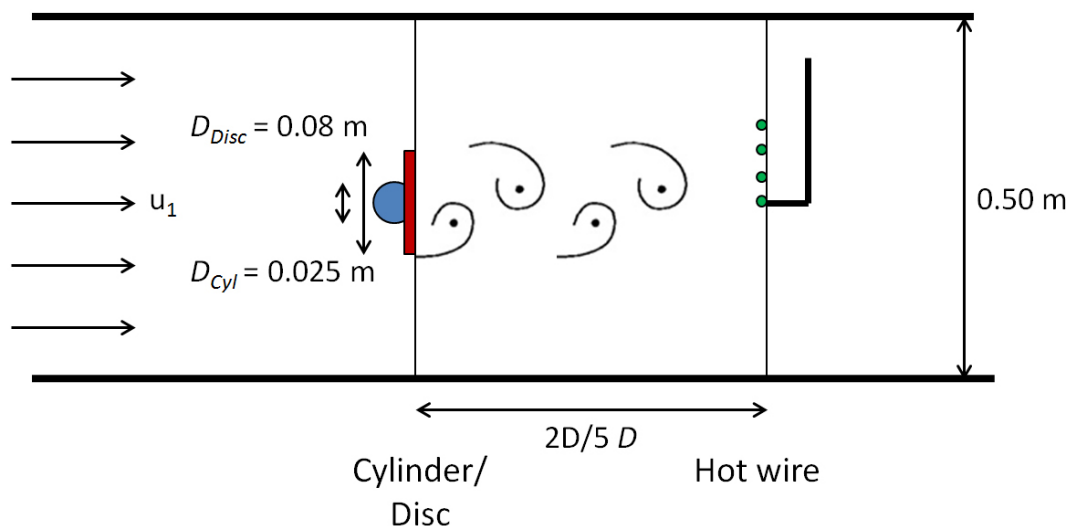


Figure 4.12: Wind tunnel arrangement for vortex shedding analysis

This experiment is done in the small wind tunnel. The set-up is similar to the first experiment in section 4.2 and can be seen in figure 4.12. A hot wire anemometer is used, to be able to measure the high frequent vortices and turbulences behind the bodies. The pitot tube will be used to calibrate the hot wire measurements. The cylinder is again fixed in about the middle of the wind tunnel. The big discs from the previous experiment are downscaled to 80 mm. They are fixed on a 230 mm long stand, which is fixed in about the

CHAPTER 4. EXPERIMENTAL RESULTS

middle of the wind tunnel to the ground.

The wind velocities behind the cylinder, the porous biplane and circular full disc are recorded at 4 different points behind the bodies each in $2 D$ and $5 D$ distance. Three of the measurement points are directly behind the bodies or behind the body edge. One point is taken outside of the direct wake flow. With regard on section 4.1.2 is assumed that the cylinder vortices are lower than 200 Hz. To reduce the aliases, which are incorrect frequencies, is a 400 Hz filter used. Wheeler and Ganji [28] recommend to have a sample frequency, at least twice the expected phenomena frequencies. But better is even a higher frequency, thus is a sampling frequency of 1000 Hz over 10 s chosen. [28, 112 ff]

4.4.3 Results

The hot wire calibration is done in the empty wind tunnel. The determined resistances are given in table 4.4. The operational resistance and the response frequency were found to be 10.5Ω and 8547 Hz.

Table 4.4: Hot wire calibration and set-up

$R_{w,c}$	5.7 Ω
R_{tot}	6.5 Ω
R_{an}	7.3 Ω
R_{op}	10.5 Ω
t_{resp}	90 μs
f	8547 Hz

The sampled data from the hot wire anemometer is analysed with a Matlab program. The program performs a discrete Fourier transformation and a power spectral density analysis to figure the main frequencies and their power density out. It is expected to see discrete frequencies that occur more often than others.

For all bodies was the position behind the edge and in $5 D$ distance giving the best results for the power spectral density analysis. That is why only the hot wire data for this position is presented in the following:

Cylinder Measurements

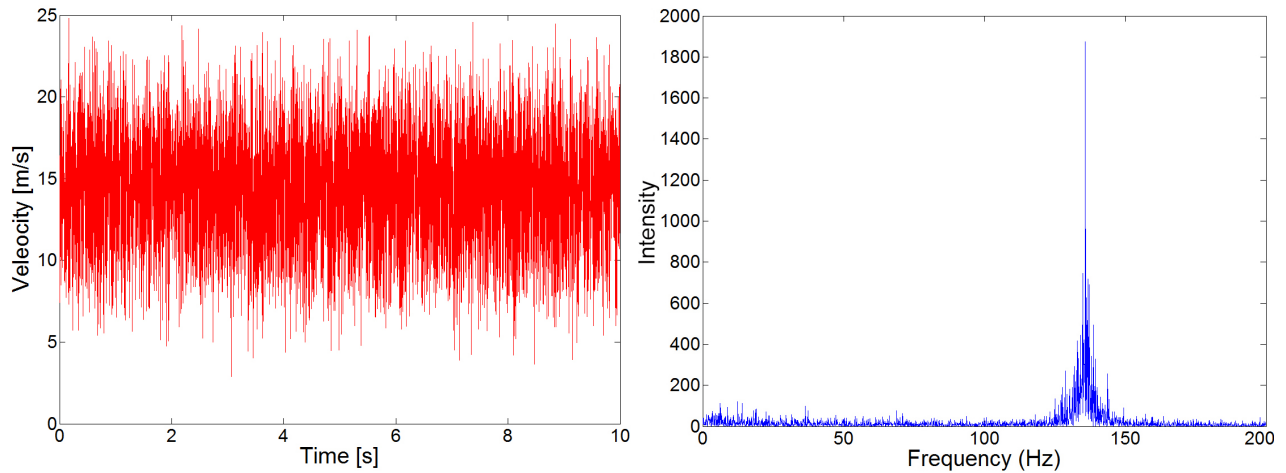


Figure 4.13: Time series (left) and power spectral density (right) for the cylinder

The time series recorded in the cylinder wake can be seen in the left diagram in figure 4.13. The measured velocities are in a wide range between 5 m/s and 25 m/s, oscillating around an average velocity of about 15 m/s. The mean velocity measured with the pitot tube is about 17.5 m/s and higher than the average hot wire measured velocity. This can be a deceleration of the flow in the wake of the cylinder. The wide spread measured velocities indicate a high turbulent flow behind the cylinder. As presented in section 2.4, it is well known, that cylinders have vortices with discrete frequencies. The vortex frequency for 17.5 m/s, estimated likewise like in section 4.1.2 is about 140 Hz. The power spectral density analysis can be seen in 4.13 on the right side. The peak at 135.8 Hz shows the frequency with the highest occurrence and is the vortex frequency of the cylinder. That can also be detected at other measure points in the wake flow. The measured vortex frequencies are in a good approach to the estimated vortex frequencies. The peaks at higher and lower frequencies are a result of noise and can have their source both in the flow measurement and in the electrical system.

The cylinder measurements show, that this method is suitable to measure vortices behind bodies. The hot wire is fast enough to measure high turbulent flows. Also the Fourier transformation and the power spectral density analysis implemented in the Matlab program are sufficient to identify the vortex frequencies.

Porous Biplane Disc Measurements

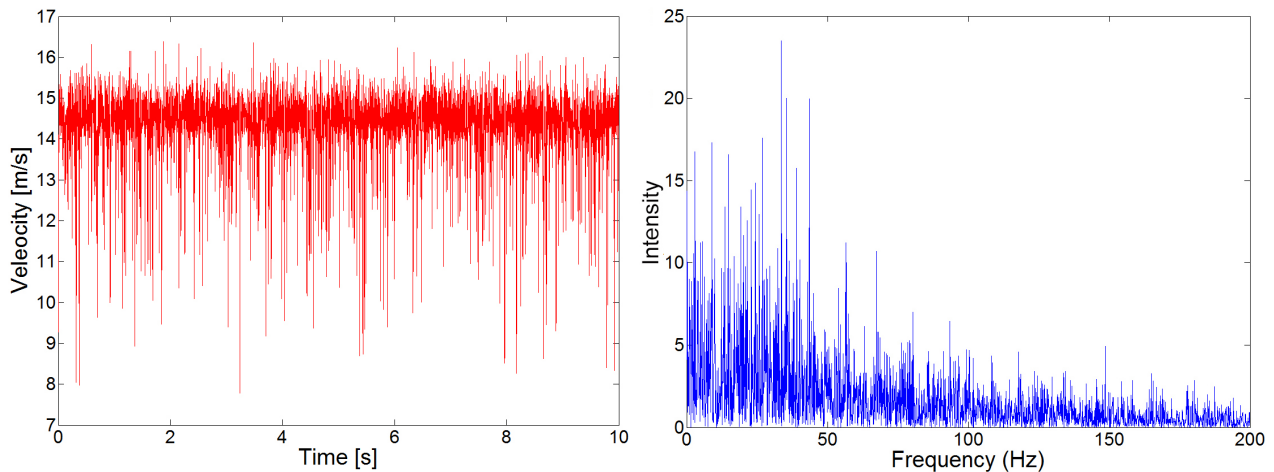


Figure 4.14: Time series (left) and power spectral density (right) for the porous biplane disc

The data is adequate generated and analysed as for the cylinder. The time series can be seen in the left diagram of figure 4.14. The measured velocities oscillate around an average velocity of about 14.5 m/s and are in a smaller range with 8 m/s to 16 m/s, than for the cylinder. The average speed is again 17.5 m/s. The lower speed behind the disc was also measured in the static measurements in section 4.3.

The power spectral density analysis on the right side of figure 4.14 shows no discrete vortex frequency. But it can be seen that most of the predominant frequencies appear in a range up to 70 Hz. The highest peaks can be found around 40 Hz. The wake flow is comprising a great many of vortex frequencies between 1 Hz and 70 Hz. In this case it is not possible to find the boarder between noise and existing vortex frequencies.

Circular Full Disc Measurements

The sampled time series on the left side in figure 4.15 shows a velocity range between 4 m/s and 18 m/s. As for the previous bodies is the inlet flow 17.5 m/s, but the time series is oscillating around an average velocity of 13 m/s.

The power spectral density diagram in figure 4.15 has a peak at 27.4 Hz. The peak has a wider basis and some noise nearby. The noise and the wider basis could be a result of a

CHAPTER 4. EXPERIMENTAL RESULTS

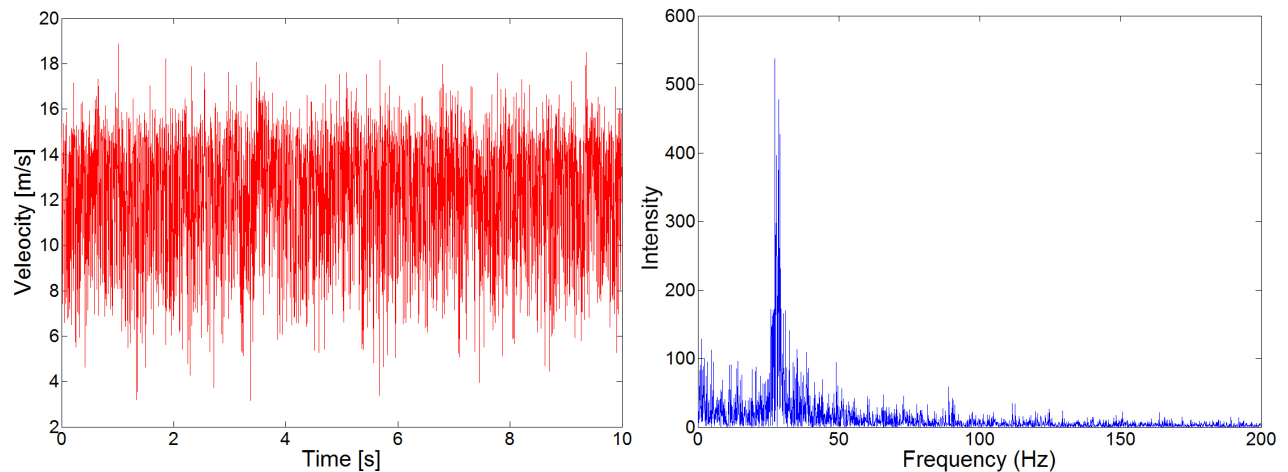


Figure 4.15: Time series (left) and power spectral density (right) for the circular full disc strong turbulence behind the disc.

Cannon et al. [6] also investigated the wake flow of circular full discs and found a Strouhal number of 0.15. In the following is the Strouhal number for this experiment with equation 2.2 determined:

$$St = \frac{f \cdot D}{u} = \frac{27.4 \text{ Hz} \cdot 0.08 \text{ m}}{17.5 \text{ m/s}} = 0.125$$

The found Strouhal number of 0.125 is similar to the 0.15 determined by Cannon et al. [6].

4.4.4 Conclusions

Vortices with discrete frequencies were found in the wake of the cylinder and the circular full disc. The cylinder has a dominant vortex frequency close to the theoretical calculated value. Also the Strouhal number of the circular full disc determined in the experiment is close to the given numbers by Cannon et al. [6]. Contrary the spectral density analysis for the porous biplane disc gave no feasible results. The highest peaks are around the same area like the one from the circular full disc. But no discrete vortex frequency can be identified, due to the existence of many peaks.

Furthermore a power spectral density analysis of the wake behind the porous monoplane disc would be interesting, although the porous discs have similar shapes. Also investigations with the big discs in the big wind tunnel could bring different results.

4.5 Error analysis

There are two different kind of measurement errors. On the one hand the random errors and on the other hand the systematic errors. Random errors are unpredictable and occur for example in measurement instruments and from fluctuation of physical conditions. They can be quantified by repeating the measurements. The systematic errors are so called built-in errors in measurements and calibration set-ups, which can only be reduced by changing components in the measurement chain. Both random and systematic errors are combined to the total error. [26, p. 3 ff]

In the following will the appearing errors, especially for the velocity measurements with pitot tubes and hot wire anemometers be discussed. The force plate measurement system is pre-calibrated and a stand alone system, which makes it difficult to analyse.

4.5.1 Pitot Tube Measurements

The pressure and velocity measurements with the pitot tubes are influenced by a chain of errors. Most of the measurement set-ups are linked: sensors, transducers and data acquisition systems. Each part of the system is influencing the measurements and adds a deviation. The signal chain is going through a lot of steps for the pitot tube:

It starts with the pitot tube themselves, which e.g. influences the flow. The dynamic pressure is transmitted via the hose to the pressure transducer and the alcohol manometer. The volume in the hose and the measurement systems effect the transmission negative, the bigger the volume is. Especially the reaction time of the signal transmission from the pitot to the pressure transducer is getting higher. The pressure is transduced to an analogue electrical signal, which is conducted and transformed to a digital signal in the data acquisition system. These signals are set into account with the alcohol manometer data. The manometer is subjected to reading, adjustment (parallel to the ground) and wetting of surfaces (surface tension of liquids) deviation. In the following a deviation estimation is done for the manometer. The pressure aberration for 1 mm difference and a typical

CHAPTER 4. EXPERIMENTAL RESULTS

quotient of the angel of 1/5 is:

$$\Delta p = h \cdot g \cdot \rho \cdot k = 1 \text{ mm} \cdot 9.81 \text{ m/s}^2 \cdot 810 \text{ kg/m}^3 \cdot 1/5 = 1.6 \text{ Pa}$$

The pressure aberration induces a velocity discrepancy of:

$$u = \sqrt{\frac{2 \cdot \Delta p}{\rho}} = \sqrt{\frac{2 \cdot 1.6 \text{ Pa}}{810 \text{ kg/m}^3}} = 0.06 \text{ m/s}$$

When measuring velocities between 5 m/s and 10 m/s is the error 1.2 % to 0.6 %.

The influence of the accuracy A of every part of the chain can be high, but in the end can the tolerances and the deviation have a big impact due to the error propagation:

$$\prod_i^n e = e_{pitot} \cdot e_{hose} \cdot e_{transduce} \dots \cdot e_i$$

Furthermore is the density of the air, which is dependent on the temperature, important for the velocity measurements. The temperature is rising, due to the energy input by the fans and the friction, when the wind tunnels are running. The temperature changes are taken into account for the calculations. But as the temperatures are measured with thermocouples, which have a certain discrepancy of usually $\pm 1.5 \text{ K}$ or $\pm 2.5 \text{ K}$, can the calculated densities only be an approach.

Pitot tubes are in general suitable to measure turbulent flows, but the output can be wrong or differ, if the flow is highly turbulent and contains back flows. Also flows that hit the pitot tube from the side or in big angles can induce lower measured velocities. [14, p. 16]

4.5.2 Hot Wire Measurements

The hot wire measurements are linked, due to the calibration, to pitot tube measurements and some of the discrepancy sources. Mainly the air content in the hose, that connects the pitot tube with the alcohol manometer and the alcohol manometer have an influence on the velocity measurements with the hot wire anemometer.

In addition can the hot wire anemometer measure the absolute velocity, but there is no

CHAPTER 4. EXPERIMENTAL RESULTS

statement about the flow direction possible. Especially in turbulent flows can the velocity vector point in other directions than e.g. parallel to the wind tunnel flow. Turbulences are intentionally induced by the investigated bodies, but also by the pitot tube next to the hot wire. Hence it is important to have a certain distance between the pitot tube and the hot wire, to have least interaction.

The hot wire velocity measurements are also influenced by the temperature of the flow. Mostly is the air estimated to have about 20 °C. But when the wind tunnels are running for a longer time, is the temperature rising and changing the velocity results. To keep the influence of temperature changes low, should the hot wires be calibrated regularly.

The response frequency of all the used hot wire anemometers is with circa 10 kHz, about 10 times higher than the sample frequency. The acquisition set-up can sample the data much faster than for the hot wires needed. That implies, that the hot wires and the acquisition set-up are appropriate to measure high turbulent flows, like in section 4.4 described.

For the experiment in section 4.4 are most of the influences presented here neglectable. The data is basically not used to determine the velocity, but to perform a frequency analysis. The quantity of the data is not important for these kind of investigations.

4.6 Comparison of Mean Wake Flows

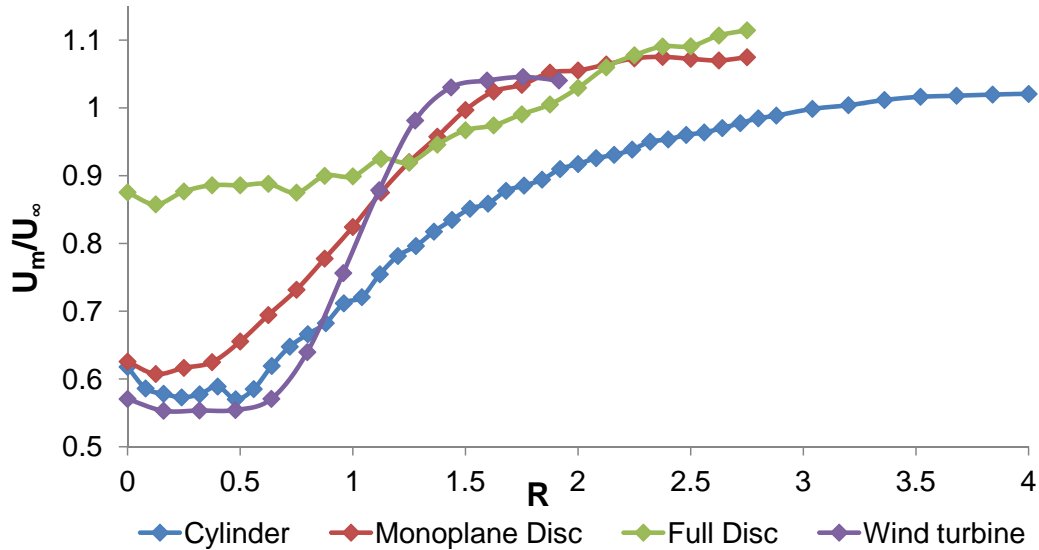


Figure 4.16: Mean wake flow comparison in $5 D$ distance of cylinder (blue), porous monoplane disc (red), circular full disc (green) and model wind turbine by Bartl [1] (purple)

The measured mean wake flows of the cylinder, the porous monoplane and the circular full disc determined in the experiments in section 4.2 and 4.3 will be compared to a model wind turbine mean wake flow measured by Bartl [1]. The graphs are plotted in 4.16.

The cylinder mean wake flow is wider, and the side has a smaller gradient than the turbine mean wake flow. The lowest flow behind the cylinder and the turbine is almost the same. But the influence of the cylinder goes further to the outside and the flow normalizes in contrast to $1.5 D$ distance for the model wind turbine at $4 D$ distance from the center.

A better result for comparing the shape can be seen for the porous monoplane disc and the model wind turbine. The gradient for the disc is smaller and the center wake flow higher. The lowest flow velocity is directly behind the disc and ends at $0.5 D$, which is earlier than for the turbine. The highest velocity on the side of the mean wake flow is reached at $1.5 D$ distance, which is a little bit further than for the model wind turbine.

The mean wake flow of the circular full disc and the model wind turbine have almost no similarity. The lowest velocity behind the disc is clearly higher than the velocity behind the

CHAPTER 4. EXPERIMENTAL RESULTS

turbine. Also the gradient towards the outside is much smaller.

None of the investigated structures have a similar shaped mean wake flow curve like a wind turbine. But the porous monoplane disc might be able to give depending on the experimental requirements satisfying results. For the simulation of wind turbine mean wake flows need more investigations with computational fluid dynamic models as well as with wind tunnel experiments to be done.

Chapter 5

Summary and Conclusions

The goal of this Master thesis was to investigate mean wake flow velocities, drag coefficients and vortex shedding frequencies in the wake flow behind cylinders and circular discs. The literature research showed that cylinder measurements can work as reference to validate the experimental set-up. Mean wake flow references were also found for the porous monoplane and the circular full disc. A mean wake flow of a model wind turbine was presented. Two different methods were introduced to determine the drag coefficient. The drag measurement by wake method requires the inlet velocity and the velocity distribution behind the bodies (mean wake flow). Whereas the force survey method demands the drag forces directly. The drag coefficient can be calculated with the drag force, as shown in equation [2.5](#).

Information about vortex shedding was found for the cylinder and the circular full disc. The literature states, that vortices with discrete frequencies appear behind cylinders and circular full discs.

The experiments were done in two NTNU wind tunnels. Appropriate sensors and measurement set-ups were presented. The forces were measured with a force plate. Two different measurement set-ups were used to measure the wind velocities. The pitot tube was used to measure the mean wake flows and to calibrate the hot wire anemometer. The velocity time series of the body wakes were recorded with a hot wire anemometer. The experimental trials included the investigation of a cylinder, a porous monoplane and

CHAPTER 5. SUMMARY AND CONCLUSIONS

a biplane disc and three circular full discs of different size.

The experimental trials conducted in this thesis had three main objectives:

1. Measurements of drag forces and mean wake velocities
2. Comparison of the drag measurement by wake and force survey method
3. Assessment of vortex shedding frequencies in cylinder and disc wakes

The first experiment was investigating the mean wake flow of a cylinder. It was performed to prove, that the measurement set-up is capable for mean wake flow measurements. Although the results were not totally conform with the literature, the experiment showed that the experimental set-up and the measurement by wake method is suitable for the determination of mean wake flows and drag coefficients. Additionally it was found that the measurement by wake method is sensitive. The results are strongly dependent on the inlet or to the asymptotic velocity.

In the second experiment was the measurement set-up extended by using a force plate to additionally use the force survey method. This experiment was performed in the big wind tunnel. Measurements were done for the porous monoplane and two different sized circular full discs. The measured mean wake flow and the drag coefficients of the porous monoplane disc are conform with the literature prediction. Contrary to the determined drag coefficients from the force survey method for the big circular full disc, is different from the literature. Due to the consideration of the blockage effect causing a deviation, a smaller circular full disc was investigated. The results for the small discs are similar to the literature.

The third and last experiment was done with a hot wire anemometer. The velocity time series of the wake flow behind the bodies were recorded in the small wind tunnel. Analytical solutions of the velocity time series resulted in the power spectral density diagrams. The diagrams for the cylinder and the circular full disc show peaks at discrete vortex frequencies, which match with the literature. No discrete vortices were found in the wake of the

CHAPTER 5. SUMMARY AND CONCLUSIONS

porous biplane disc.

Furthermore all the mean wake flows measured in the experiments were compared to the results of a model wind turbine. Not one of the body wakes fit good with the flow behind the turbine, whereas the circular full disc has the least analogy. The wake velocities are clearly higher and the cylinder wake fits directly behind the cylinder. Outside of the direct wake the gradient is low and the flow normalises far away from the direct cylinder wake. The best conformity is given by the mean wake flow of the porous monoplane disc. Nevertheless the flow behind the disc is higher and the gradient towards the edge is smaller.

In this early stadium of research, it is not easy to conclude, that porous and circular disc measurements are adequate for wind turbine wake modelling. Further wind tunnel and CFD investigations need to be done to approve similar wake flow behaviour for discs and wind turbines. A CFD analysis for discs and wind turbines was done by Bosio [2]. Comparisons between CFD and wind tunnel analysis are a major step to verify the wake models. It seems that the mean wake flows of porous discs are promising to simulate wind turbine wake flows. Future investigations could focus on the influence of a mesh grid porosity variability for the mean wake flow of the discs. Additionally a comparison of the mean wake flows revealed a significant variation between shape of the cylinder and discs to the model wind turbine. This however, show that the porous monoplane disc achieved the best results and is therefore most promising for future investigations on wind turbine wake modelling.

Appendix A

Additional tables

Table A.1: Pressure and velocity in cylinder wake

Position [mm]	p_{dyn} [Pa]	u [m/s]	Position [mm]	p_{dyn} [Pa]	u [m/s]
100	131.1	14.8	31	113.6	13.7
95	130.5	14.7	30	112.0	13.6
90	129.8	14.7	29	111.3	13.6
85	128.8	14.6	28	108.5	13.4
80	128.0	14.6	27	106.8	13.3
75	127.4	14.5	26	105.6	13.2
70	127.0	14.5	25	103.7	13.1
65	126.7	14.5	24	102.0	13.0
62	126.7	14.5	23	98.5	12.8
59	126.9	14.5	22	96.6	12.7
56	127.3	14.5	21	94.9	12.6
53	127.8	14.6	20	90.9	12.3
50	128.4	14.6	19	89.3	12.2
48	128.1	14.6	18	85.9	11.9
46	127.7	14.6	17	82.3	11.7
44	127.3	14.5	16	78.1	11.4
42	126.1	14.5	15	75.3	11.2
40	124.2	14.4	14	70.2	10.8
38	122.9	14.3	13	64.0	10.3
36	120.5	14.1	12	62.4	10.2
35	119.5	14.1	11	57.4	9.8
34	117.7	14.0	10	54.7	9.5
33	116.0	13.9	9	51.7	9.3
32	114.5	13.8	8	47.2	8.9

APPENDIX A. ADDITIONAL TABLES

Table A.2: Pressure and velocity in cylinder wake

Position [mm]	p_{dyn} [Pa]	u [m/s]	Position [mm]	p_{dyn} [Pa]	u [m/s]
7	42.2	8.4	-24	112.8	13.7
6	40.0	8.2	-25	114.0	13.8
5	42.7	8.4	-27	115.9	13.9
4	41.1	8.3	-28	117.0	13.9
3	40.4	8.2	-29	118.5	14.0
2	41.2	8.3	-30	119.2	14.1
1	42.3	8.4	-31	121.1	14.2
0	47.0	8.8	-32	121.6	14.2
-1	48.4	9.0	-33	122.7	14.3
-2	51.6	9.3	-34	123.2	14.3
-3	58.0	9.8	-35	123.5	14.3
-4	60.7	10.0	-36	124.5	14.4
-5	61.7	10.1	-38	125.5	14.4
-6	66.6	10.5	-40	125.3	14.4
-7	70.6	10.8	-42	125.6	14.4
-8	75.0	11.2	-44	125.7	14.5
-9	77.1	11.3	-46	125.0	14.4
-10	81.6	11.6	-48	124.6	14.4
-11	84.9	11.9	-50	124.6	14.4
-12	87.4	12.0	-53	123.9	14.3
-13	90.8	12.3	-56	123.7	14.3
-14	94.2	12.5	-59	123.6	14.3
-15	97.2	12.7	-62	123.4	14.3
-16	99.8	12.9	-65	123.3	14.3
-17	100.9	12.9	-70	123.5	14.3
-18	102.7	13.1	-75	123.5	14.3
-19	104.7	13.2	-80	123.5	14.3
-20	106.0	13.3	-85	124.0	14.4
-21	108.0	13.4	-90	124.4	14.4
-22	109.5	13.5	-95	124.8	14.4
-23	110.8	13.6	-100	124.8	14.4

APPENDIX A. ADDITIONAL TABLES

Table A.3: Pressure and velocity in the horizontal wake of the porous monoplane and full drag disc

Position [mm]	Drag Disc		Monoplane Disc	
	p_{dyn} [Pa]	u [m/s]	p_{dyn} [Pa]	u [m/s]
0	57.6	10.0	29.4	7.1
50	55.3	9.8	27.7	6.9
100	57.7	10.0	28.5	7.0
150	59.0	10.1	29.3	7.1
200	59.0	10.1	32.2	7.5
250	59.2	10.1	36.2	7.9
300	57.5	10.0	40.2	8.3
350	60.8	10.3	45.4	8.9
400	60.7	10.2	51.0	9.4
450	64.2	10.5	57.4	10.0
500	63.4	10.5	63.5	10.5
550	67.1	10.8	68.7	10.9
600	70.1	11.0	74.5	11.4
650	71.2	11.1	78.6	11.7
700	73.6	11.3	80.1	11.8
750	75.8	11.5	83.0	12.0
800	79.5	11.7	83.5	12.0
850	84.2	12.1	84.8	12.1
900	87.1	12.3	86.3	12.2
950	89.1	12.4	86.6	12.3
1000	89.2	12.4	86.1	12.2
1050	91.8	12.6	85.7	12.2
1100	93.0	12.7	86.5	12.3

APPENDIX A. ADDITIONAL TABLES

Table A.4: Pressure and velocity in the vertical wake of the full drag and porous monoplane disc

Drag Disc			Porous Monoplane Disc		
Position [mm]	p_{dyn} [Pa]	u [m/s]	Position [mm]	p_{dyn} [Pa]	u [m/s]
600	73.9	11.3	600	93.1	12.6
550	67.8	10.8	550	87.2	12.2
500	66.9	10.7	500	82.6	11.8
475	64.7	10.6	450	77.8	11.5
450	62.7	10.4	400	72.3	11.1
425	60.9	10.2	350	66.1	10.6
400	59.7	10.1	300	59.2	10.0
380	57.2	9.9	250	51.9	9.4
360	58.1	10.0	200	45.9	8.8
340	57.9	10.0	150	40.4	8.3
320	57.3	9.9	100	35.4	7.8
300	56.4	9.9	50	30.7	7.2
250	57.9	10.0	0	28.5	7.0
200	54.0	9.6	-50	27.3	6.8
100	56.9	9.9	-100	28.0	6.9
0	55.9	9.8	-150	28.9	7.0
-100	55.6	9.8	-200	32.2	7.4
-200	54.7	9.7	-250	36.3	7.9
-250	55.1	9.7	-300	40.4	8.3
-300	54.5	9.7	-350	44.2	8.7
-320	54.9	9.7	-400	49.0	9.1
-340	55.5	9.8	-450	53.8	9.6
-360	54.7	9.7	-500	58.2	10.0
-380	57.0	9.9	-550	62.7	10.3
-400	56.2	9.8	-600	67.0	10.7
-425	57.3	9.9	-700	70.0	10.9
-450	54.2	9.7	-800	72.8	11.1
-475	56.4	9.9	-900	55.4	9.7
-500	57.3	9.9			
-550	59.9	10.2			
-600	61.5	10.3			
-700	62.5	10.4			
-800	59.4	10.1			
-900	43.0	8.6			

Bibliography

- [1] J. Bartl. Wake measurements behind an array of two model wind turbines. Master's thesis, Norwegian University of Science and Technology, 2011.
- [2] F. Bosio. Evaluation of predictive methods for wind turbine performance and wake development. Master's thesis, Politecnico Di Torino, 2014.
- [3] BP. Wind energy, access January 2014. URL www.bp.com/en/global/corporate/about-bp/energy-economics/statistical-review-of-world-energy-2013/review-by-energy-type/renewable-energy/wind-energy.html.
- [4] G. Bruschi, T. Nishioka, K. Tsang, and R. Wang. A comparison of analytical methods drag coefficient of a cylinder. 2003.
- [5] S. C. Cannon. *Large-scale structures and the spatial evolution of wakes behind axisymmetric bluff bodies*. PhD thesis, The University of Arizona, 1991.
- [6] S. C. Cannon, E. Champagne, and A. Glezer. Observations of large-scale structures in wakes behind axisymmetric bodies. *Experiments in Fluids*, 1993.
- [7] Engineering Sciences Data Unit. Characteristics of atmospheric turbulence near the ground - ESDU 74031, 1974.
- [8] K.-H. Grote and J. Feldhusen. *Dubbel - Taschenbuch für Maschinenbau*. Springer Verlag, 21. edition, 2005.
- [9] P.-Å. Krogstad and P. E. Eriksen. "Blind test" calculations of the performance and wake development for a model wind turbine. 2012.

BIBLIOGRAPHY

- [10] E. Kulunk. *Aerodynamics of Wind Turbines, Fundamental and Advanced Topics in Wind Power*. 2011.
- [11] J. F. Manwell, J. G. McGowan, and A. L. Rogers. *Wind Energy Explained - Theory, design and application*. John Wiley & Sons Ltd., 2. edition, 2009.
- [12] R. Mikkelsen. *Actuator Disc Methods Applied to Wind Turbines*. PhD thesis, Technical University of Denmark, 2003.
- [13] J. Nedic, B. Ganapathisubramani, and J. C. Vassilicos. Drag and near wake characteristics of flat plates normal to the flow with fractal edge geometries. 2013.
- [14] W. Nitsche and A. Brunn. *Strömungsmesstechnik*. Springer-Verlag, Berlin Heidelberg, 2. edition, 2006.
- [15] H. Oertel, M. Böhle, and U. Dohrmann. *Strömungsmechanik*. Vieweg + Teubner, GWV Fachverlage GmbH, Wiesbaden, 5. edition, 2009.
- [16] L. Ong and J. Wallace. *Experiments in Fluids*. Springer-Verlag, 1996.
- [17] F. Pierella and L. R. Sætran. Effect of initial conditions on flow past grids of finite extension. 2010.
- [18] F. Pierella, P.-Å. Krogstad, and L. Sætran. Blind test 2 calculations for two in-line model wind turbines where the downstream turbine operates at various rotational speeds. 2014.
- [19] V. Quaschnig. *Regenerative Energiesysteme*. Hanser, 7. edition, 2011.
- [20] G. Robertson, G. Caldwell, J. Hamill, G. Kamen, and S. Whittlesey. *Research Methods in Biomechanics*. Human Kinetics, 2. edition, 2014.
- [21] G. B. Salem and M. K. Ibrahim. Drag measurement on cylindrical bodies by wake survey method. 2004.
- [22] H. Schlichting and K. Gersten. *Grenzschicht-Theorie*. Springer Verlag, 10. edition, 2006.

BIBLIOGRAPHY

- [23] T. Schütz. *Hucho - Aerodynamik des Automobils: Strömungsmechanik, Wärmetechnik, Fahrdynamik, Komfort*. Springer, 6. edition, 2013.
- [24] H. Sigloch. *Technische Fluidmechanik*. VDI-Verlag, 7. edition, 2009.
- [25] B. M. Sumer and J. Fredsoe. *Hydrodynamics Around Cylindrical Structures*. 1997.
- [26] J. R. Taylor. *An Introduction to Error Analysis*. University Science Books, 1997.
- [27] Verein Deutscher Ingenieure VDI. *VDI Wärmeatlas*. Berlin Heidelberg, 10. edition, 2006.
- [28] A. J. Wheeler and A. R. Ganji. *Introduction to Engineering Experimentation*. Pearson Education, 3. edition, 2010.
- [29] F. M. White. *Fluid mechanics*. McGraw-Hill International, 6. edition, 2008.